



MSU Graduate Theses

Spring 2018


Magnetic Anisotropy and Exchange Bias in L1₀ FePt/NiO Bilayer Thin Films

Zachary B. Leuty

Missouri State University, zbl1@live.missouristate.edu

As with any intellectual project, the content and views expressed in this thesis may be considered objectionable by some readers. However, this student-scholar's work has been judged to have academic value by the student's thesis committee members trained in the discipline. The content and views expressed in this thesis are those of the student-scholar and are not endorsed by Missouri State University, its Graduate College, or its employees.

Follow this and additional works at: <https://bearworks.missouristate.edu/theses>

 Part of the [Condensed Matter Physics Commons](#), [Engineering Physics Commons](#), and the [Plasma and Beam Physics Commons](#)

Recommended Citation

Leuty, Zachary B., "Magnetic Anisotropy and Exchange Bias in L1₀ FePt/NiO Bilayer Thin Films" (2018).

MSU Graduate Theses. 3262.

<https://bearworks.missouristate.edu/theses/3262>

This article or document was made available through BearWorks, the institutional repository of Missouri State University. The work contained in it may be protected by copyright and require permission of the copyright holder for reuse or redistribution.

For more information, please contact bearworks@missouristate.edu.

**MAGNETIC ANISOTROPY AND EXCHANGE BIAS IN L1₀ FePt/NiO BILAYER
THIN FILMS**

A Masters Thesis

Presented to

The Graduate College of

Missouri State University

In Partial Fulfillment

Of the Requirements for the Degree

Master of Science, Materials Science

By

Zachary B. Leuty

May 2018

Copyright 2018 by Zachary B. Leuty

MAGNETIC ANISOTROPY AND EXCHANGE BIAS IN L1₀ FePt/NiO BILAYER THIN FILMS

Physics, Astronomy, and Materials Science

Missouri State University, May 2018

Master of Science

Zachary B. Leuty

ABSTRACT

Perpendicular exchange bias (PEB), particularly when it persists in nanomaterials to room temperature, is highly useful for applications in spintronic devices and for advancing the development of high-information-density magnetic random access memory. A complete mechanistic and theoretical understanding of exchange bias has evaded scientists. The quest to discover novel materials for magnetic and spintronic device applications has stimulated investigation into nanomaterials having optimal and/or tailored magnetic properties that are based on the exchange bias effect. In this study, pulsed laser deposition was used to grow epitaxial PEB systems of ferromagnetic FePt thin film layers that are interfaced with antiferromagnetic NiO thin film layers. Different phases of FePt were grown on a single crystal MgO substrate and overlain with NiO in order to investigate the exchange bias effect between the two magnetic layers. The magnetic ordering and spin-spin interactions at the FePt-NiO thin film interface results in the orthogonal/perpendicular exchange bias due to the magnetocrystalline anisotropy of FePt and orientation of the NiO antiferromagnetic planes. Using XRD, TEM, HAADF imaging, and TEM-FFT analyses, it was determined that the FePt and NiO layers were grown epitaxially on the (100) surface of the MgO substrate. HAADF imaging and TEM-EDS confirm the thin films have minimal diffusion between the layers. SQUID magnetometry data measured from the thin film samples in both in-plane and out-of-plane orientations show that the chemical ordered L1₀ FePt exhibits PEB effects.

KEYWORDS: Epitaxy, Magnetocrystalline Anisotropy, Perpendicular Exchange Bias, Iron Platinum, High Density Recording Media, Magnetic Random Access Memory

This abstract is approved as to form and content

Robert Mayanovic, PhD
Chairperson, Advisory Committee
Missouri State University

**MAGNETIC ANISOTROPY AND EXCHANGE BIAS IN L1₀ FePt/NiO BILAYER
THIN FILMS**

By

Zachary B. Leuty

A Masters Thesis
Submitted to the Graduate College
Of Missouri State University
In Partial Fulfillment of the Requirements
For the Degree of Master of Science, Materials Science

May 2018

Approved:

Robert Mayanovic, PhD

Kartik Ghosh, PhD

Fei Wang, PhD

Julie Masterson, PhD: Dean, Graduate College

In the interest of academic freedom and the principle of free speech, approval of this thesis indicates the format is acceptable and meets the academic criteria for the discipline as determined by the faculty that constitute the thesis committee. The content and views expressed in this thesis are those of the student-scholar and are not endorsed by Missouri State University, its Graduate College, or its employees.

ACKNOWLEDGEMENTS

I would like to dedicate this thesis to all of those who have supported me throughout my life. The tremendous guidance and assistance from the PAMS faculty and staff at Missouri State University has given me the tools and opportunities to learn and apply the knowledge present in this thesis.

I would like to thank Dr. Robert Mayanovic immensely for his great help and patience throughout this process. His guidance and expertise has inspired me to devote many hours, days and nights into the work present in this thesis. He continues to push me every day to explore my full potential. Thank you Dr. M for this amazing opportunity.

I would like to dedicate this thesis to the love of my life, Julia Sabina Barile.

TABLE OF CONTENTS

Overview.....	1
Investigations of the Magnetic Perpendicular Exchange Bias in L1 ₀ FePt/NiO Bilayer Thin Films	5
Abstract.....	5
Introduction.....	6
Experimental Details.....	7
Results & Discussion	9
X-ray Diffraction (XRD)	9
Transmission Electron Microscopy (TEM)	10
SQUID Magnetometry.....	12
Conclusion	14
Acknowledgments.....	15
References.....	15
Magnetic and Structural Study of Perpendicular Magnetic Anisotropy in L1 ₀ FePt/NiO Bilayer Thin films	16
Abstract.....	16
Introduction.....	16
Experimental	18
Results & Discussion	19
X-ray Diffraction (XRD)	19
High Angle Annular Dark Field Imaging (HAADF).....	22
Energy Dispersive X-ray Spectroscopy Mapping (EDS)	23
Fast-Fourier Transform of TEM micrograph (FFT-TEM)	28
X-Ray Reflectivity (XRR)	30
SQUID Magnetometry.....	33
Conclusions.....	40
References.....	40
Summary	43

LIST OF TABLES

Table 1. Deposition growth parameters for thin film bilayer types A and B. In the pressure column, the atmosphere is also noted.9

LIST OF FIGURES

Figure 1. XRD of sample A. Sample B showed an identical XRD pattern. The legend indicates peaks from the MgO substrate	10
Figure 2. A high magnification TEM image of the cross-sectioned bilayer of sample A .11	
Figure 3. A FFT of Figure 2. Note the symmetry of the NiO (111) along the vertical axis and the epitaxial periodicity of the FePt spots along the vertical and horizontal axis.....	12
Figure 4. SQUID magnetometer data of sample A Sample B. Sample A exhibits soft-ferromagnetic properties. Sample B exhibits hard-ferromagnetic properties.	14
Figure 5. XRD Measurements of Sample B. This Shows the epitaxial nature of the L1 ₀ FePt layer and the highly oriented NiO layer. The XRD for film type A looks very similar to this figure.	20
Figure 6. XRD measurements of the film type C. The FePt (200) peak is the A1 phase ..	21
Figure 7. HAADF image of film type A. The bright island are L1 ₀ FePt while the material on top of this is the highly oriented NiO. Not the scale bar on the right.	23
Figure 8. EDS of the sample type A. Note the difficulty in resolution even with the drastically different colored elements	25
Figure 9. The separated images of figure 8 (sample A). Note the FePt island seen in the middle images	26
Figure 10. High-resolution TEM Micrograph of Sample type A. Note the grains/islands of FePt and the NiO crystalline dislocations. The scale length bar is 10 nanometers	27
Figure 11. Fast-Fourier transform of Figure 10 high-resolution micrograph	29
Figure 12. The separated FFT of the High-magnification TEM micrograph from sample A.....	30
Figure 13. XRR of Sample A. The experimental data is in red, the calculated XRR pattern is in blue and the residual signal is in grey	31
Figure 14. The density ditribution function of film type A calculated from the XRR diffracted intensities peaks.....	32

Figure 15. The block diagram of film A with quantified properties calculated from the XRR experimental measurement. This includes film thickness, density, and surface roughness	32
Figure 16. Magnetic M-H hysteresis loop of film A in the in-plane orientation	36
Figure 17. Magnetic M-H hysteresis loop of film A in the out-of-plane orientation	36
Figure 18. Magnetic M-H hysteresis loop of film B in the in-plane orientation	37
Figure 19. Magnetic M-H hysteresis loop of film B in the out-of-plane orientation.....	37
Figure 20. Magnetic M-H hysteresis loop of film C in the in-plane orientation	38
Figure 21. Magnetic M-H hysteresis loop of film C in the out-of-plane orientation.....	38

OVERVIEW

The discovery of electricity, magnetism and electromagnetic theories has pioneered the revolution of technology in our everyday lives. Much of today's technology is based on the laws of electricity and magnetism to result in a powerful and useful tool. As society advances, so does the technology allowing for simplification of processes that were once complicated and required much more time to complete. This acceleration and advancement in technology has created a very high demand for more advanced technologies. This is why the semiconductor industry is the largest and most profitable industry in the entire world. Electronics have become a requirement to perform even simple tasks that were once only done by pencil and paper. This demand requires technology to continually advance, creating faster and smaller electronics than the previous generation. This world wide challenge calls on any and all scientists in the field to offer their dedication to solving such complicated problems. This thesis is my contribution to the scientific community to help generate creative solutions for such technological challenges.

Magnetic recording has long been the industry standard for storing large amounts of data in a reliable fashion that does not require a constant power source to retain the stored information. Despite advances such as flash memory, magnetic recording media is still predominantly used in storing high quantities of data. This is due to the relatively low cost in storing information in magnetic recording media. Data centers that store cloud information, such as Google or Microsoft, have facilities dedicated to store large industrial computer racks that contain only computer hard disk drives for the sole purpose of

storing all of the data they possess. The computer hard disk drives that are used for cloud storage work from the exact same principle and have a similar design to hard disk drives available for consumer purchase. For the last couple of decades, perpendicular magnetic recording has been the industry standard for hard disk drives due to the higher density of storage per square inch compared to that of parallel magnetic recording. Unfortunately, perpendicular magnetic recording is approaching its theoretical storage density limit and a new magnetic recording technique must take its place as the industry work horse in information storage. There are several options to that offer higher magnetic recording storage densities but many of them require a very large initial investment in infrastructure required to mass produce such media. Heat assisted magnetic recording (HAMR) is projected to be the next industry leader in the near future magnetic recording design. It is more cost efficient for the industry to adopt, implement and mass produce HAMR than other designs such as bit patterned media. Although there are many challenges that come with this recording technique, many of them have been surmounted and HAMR will be introduced into the market and mass produced within several years of the publishing of this thesis. Industry leading companies have released preliminary models of the drives for reliability testing showing the technology is not so far away.

One of the most promising materials for use in HAMR drives is iron platinum (FePt), more specifically the $L1_0$ phase of FePt. I decided to work with this material to see if it also had potential applications in other areas or in the form of different device designs. Exchange bias is an important phenomenon for applications in magnetic random access memory (MRAM), spin valves and other spintronic devices. This concept led to the study described in this thesis of the exchange bias in $L1_0$ FePt/NiO thin films. $L1_0$

FePt is a ferromagnetic material and in order to induce exchange bias, an antiferromagnetic material must be grown in contact with the ferromagnetic layer to achieve spin-spin exchange coupling at the interface of the two materials. While selecting an antiferromagnetic material, several important factors must be considered. These factors include epitaxial relationship, Néel temperature, antiferromagnetic ordering, diffusion between the materials and the strength of the antiferromagnetic material or its exchange interaction. These considerations lead to the selection of nickel oxide (NiO) as the antiferromagnetic material because it scores well in many of these categories. Most importantly, the Néel temperature of NiO is much higher than room temperature giving the possibility of room-temperature exchange bias, a desirable property for devices. Another important reason for selecting these materials is the epitaxial relationship of L1₀ FePt and NiO lead to perpendicular exchange bias. This is due to the magnetic moment orientations in both materials at the interface, the Fe magnetic spins point orthogonal and anti-orthogonal to antiferromagnetic planes in the NiO. This is caused by the magnetocrystalline anisotropy present in the L1₀ FePt material. Perpendicular exchange bias is more desirable than traditional exchange bias for applications and fabrication of devices.

After the growth of these thin film bilayers, standard techniques were used to characterize the thin film system. This is very important to learn more about the properties of the thin film and to confirm the film consists of what is actually predicted. In this thesis, I describe how the thin films were grown and the optimization of the parameters used to obtain successful growth of the desired materials. In addition, I describe the results from the structural, morphological, elemental and magnetic

measurements used to characterize the FePt/NiO bilayer thin films. Finally, I discuss the results from the characterization of the FePt/NiO bilayer thin films in the context of potential applications and future directions for research for these materials.

INVESTIGATIONS OF THE MAGNETIC PERPENDICULAR EXCHANGE BIAS IN L₁₀ FePt/NiO BILAYER THIN FILMS

Abstract

I report on the exploration of perpendicular exchange bias in iron platinum/nickel oxide (FePt/NiO) bilayer thin films grown using pulsed laser deposition (PLD) on MgO (100) substrates. Exchange bias is an important property for giant magnetoresistance, and, as such has promise for applications in spin valves, magnetic sensors and magnetic random access memory. The magnetic L₁₀ phase of FePt is known for having high perpendicular magnetic anisotropy, tunable coercivity/grain size and large magnetic storage density. The FePt layer was first deposited directly on MgO, followed by the deposition of the NiO layer on top of the FePt layer. The coercivity of the L₁₀ FePt layer was tuned during growth to form a hard or soft magnetic layer. The FePt/NiO thin films grown for this study exhibit perpendicular exchange bias at 5K, as quantified using our SQUID measurements. XRD confirms parallel plane ordering between the MgO (200), FePt (002) and NiO (111) atomic planes while cross-sectional TEM confirms the epitaxial growth of L₁₀-FePt(001)<100>//MgO(100)<001> and the preferential growth of NiO on top of the FePt. Films of only FePt were grown to examine the surface architecture of the ferromagnetic layer and thus the interface of the FePt/NiO bilayer. The results from the XRD, TEM and magnetometry characterization of the FePt films and FePt/NiO bilayer thin films will be discussed.

Introduction

Exchange bias is generally accepted to be due to spin-spin coupling occurring at the interface between ferromagnetic (FM) and anti-ferromagnetic (AFM) layers. Although exchange bias can occur in many types of systems, it most commonly occurs in core-shell nanoparticles or layered thin films. The effect has been studied computationally and experimentally since its discovery in 1956 by Meiklejohn and Bean¹. Exchange bias has applications in magnetic storage devices, such as magnetic RAM, spin-valves, GMR and other spintronic devices. The origin of exchange bias is still debated today mainly due to various competing theories that have been offered and because there may be a number of potential mechanisms that are responsible for the effect. A leading theory for a structure with FM magnetic ordering orthogonal to the bulk AFM easy axis suggests that an incomplete domain wall is created in the FM layer leading to exchange bias (EB)². This type of system is referred to as the “Frozen Interface Model” by Kiwi *et al.* and also explains the AFM spin canting at the interface³. Calculations often overestimate the experimental exchange bias because it can be difficult to model the interface defects and other phenomena such as spin canting or coupling frustration at the FM/AFM interface. Perpendicular exchange bias (PEB) can be obtained with an epitaxial FM layer that has a magneto-crystalline uniaxial anisotropy normal to the surface of the thin film or nanocrystal. FePt is a strong candidate for PEB because of its strong magnetic anisotropy in the L1₀ phase. Perpendicular FM spin orientations, such as in PEB, allow for higher magnetic storage densities making PEB quite desirable. It has been suspected that this PEB system with orthogonal coupling may have spin canting at the FePt/NiO interface where the angle between the FM/AFM

interface spins is not exactly 90 degrees. Recently, Gao *et al.* (2016) have confirmed this small angle deviation of the Ni spins in the easy axis of a coupled L1₀ FePt/NiO bilayer⁴.

It has recently been discovered that the hardness of the magnetic hysteresis loop can be controlled by pressure and atmosphere inside the growth chamber during pulsed layer deposition (PLD) of FePt/NiO bilayers⁵. This paper presents a study comparing how different atmospheres during PLD growth affect the magnetic properties of FePt/NiO bilayers, specifically the ferromagnetic hysteresis loop hardness and the exchange bias.

Experimental Details

FePt was first PLD deposited directly on an MgO substrate, which was subsequently overlain by PLD deposition of NiO, resulting in a layered structure of MgO\FePt\NiO for all films. An Nd:YAG laser with a wavelength of 266 nm and laser fluence of 2.0 J/cm² (± 0.2 J/cm²) was used for all depositions of the thin film layers. The antiferromagnetic target was made of nickel(II) oxide (NiO) powder of 98.0% purity. The powder was ground, pressed and sintered at 1500 °C for 12 hours to form the target and confirmed to have the rocksalt structure of NiO using x-ray diffraction (XRD). The iron platinum (FePt) target was made using a Fe:Pt 50:50 at.% mixture. Metallic iron powder (99.9% purity) and platinum pellets (99.99% purity) were combined using vacuum arc melting to form a solid metallic target. Using XRD, it was confirmed that the FePt target was the chemically disordered A1 FePt phase. The substrate used for all films was single crystal MgO(100) with the deposition side EPI polished then packed in a 100 grade clean

plastic bag under 1000 grade clean room. All substrates were heated to 800 °C under high vacuum prior to deposition of the thin films.

Table 1 below shows the environmental conditions within the PLD chamber that were used to prepare the two thin film heterostructures used in this study. Whereas the conditions used to deposit the NiO film were identical, the growth pressure and atmosphere for the FePt layer were varied between thin film bilayer types A and B (see table I). The FePt layer for film A was deposited under low vacuum with a forming gas (FG) (5% H₂ & 95% Ar) atmosphere, whereas film B was deposited under high vacuum without any additional gas added. A substrate temperature of 800 °C was used to induce L₁₀ ordering in the FePt layer during deposition of the thin film. All other parameters were previously optimized and held constant for the entirety of this study. For both bilayer thin films, the substrate was cooled to 200 °C prior to the introduction of O₂ into the chamber and deposition of NiO over the FePt layer. This cooling step preserved the FePt layer from oxidation during the addition of O₂ in the vacuum chamber. XRD was measured for the substrates, targets and thin film samples using a Rigaku Smart Lab instrument at the Air Force Research Lab, and using a Bruker D8 Discover instrument, both of which are equipped with a Cu Ka-1 source. A FEI Talos F200 series microscope was used for imaging the cross section of the thin film. Magnetic hysteresis loop data were collected for the bilayers using Quantel MPMS SQUID. The field cooled (FC) hysteresis loops were measured by first cooling the samples from 300K to 5k under a magnetic field of 50kOe.

Table 1: Deposition growth parameters for thin film bilayer types A and B. In the pressure column, the atmosphere is also noted. (FG represents forming gas, a mixture of 5% H₂ and 95% Ar.)

Name	FePt Deposition			NiO Deposition		
	Temperature	Pressure	Pulses	Temperature	Pressure	Pulses
A	800 °C	1.0e-1 mbar FG	10,000	200 °C	1.3e-1 mbar O ²	25,000
B	800 °C	3.4e-6 mbar	10,000	200 °C	1.3e-1 mbar O ²	25,000

Results & Discussion

X-ray Diffraction (XRD). The XRD data measured from sample A and shown in Figure 1 provides evidence for an epitaxial registry of atomic planes of the bilayers relative to the MgO substrate. The high crystallinity and known epitaxial relationship⁴ suggests these films are both highly oriented for each layer, FePt and NiO. The presence of FePt (001), (002), and (003) reflections suggest that the layer is epitaxial with the MgO substrate. The peaks in the figure marked with an asterisk indicate crystalline plane reflections originating from the MgO substrate.

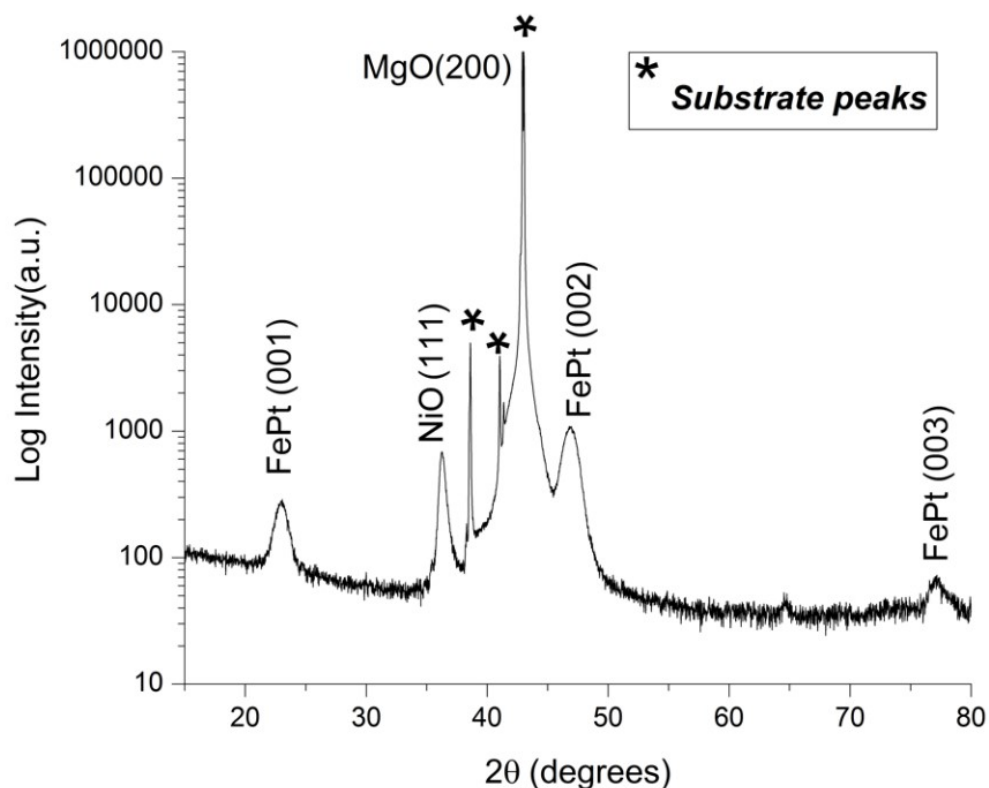


Figure 1: XRD of sample A. Sample B showed an identical XRD pattern. The legend indicates peaks from the MgO substrate

Transmission Electron Microscopy (TEM). Figure 2 shows the TEM images collected from sample A. The TEM cross section sample was prepared using focused ion beam (FIB). After the sample was thinned and attached to a copper grid, the sample was then NanoMilled to remove any amorphous gallium and to further thin the sample. Figure 2 is a low magnification image of the bilayer cross section. The respective layers are also labelled in the figure. The FePt layer is approximately 7 nm thick whereas the NiO layer is 105 nm thick. The NiO layer appears much thinner in the image because the top half was removed during the ion milling process. The FePt layer has an island like morphology. This morphology is more easily observable in the HAADF images that were collected but are not presented here. Figure 3 shows the Fast-Fourier (FFT) transform of

Figure 2, which shows the structural aspects of the sample in reciprocal space. The FFTs, which were taken of each layer individually, confirm the epitaxial growth of FePt and highly oriented growth of NiO. It is likely that NiO is also epitaxial, but the crystalline planes of this layer are not sufficiently aligned with the electron beam axis of the TEM to show this fully. FePt and NiO have an established epitaxial relationship with six-fold symmetry⁴. This gives rise to the different grain orientations seen in Figure 2.

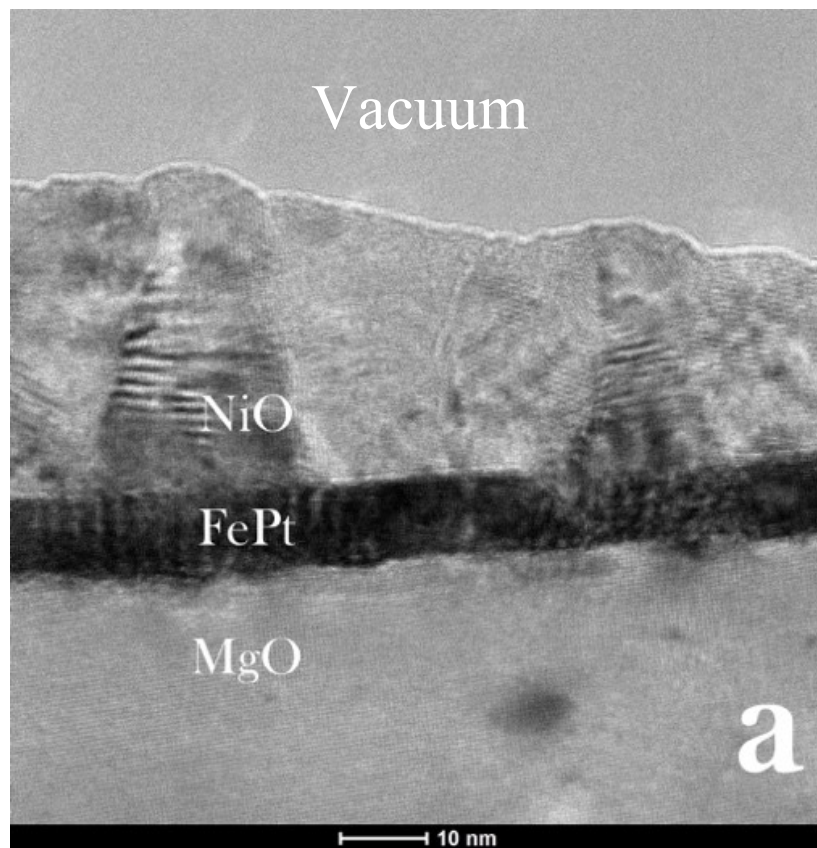


Figure 2: A high magnification TEM image of the cross sectioned bilayer of sample A

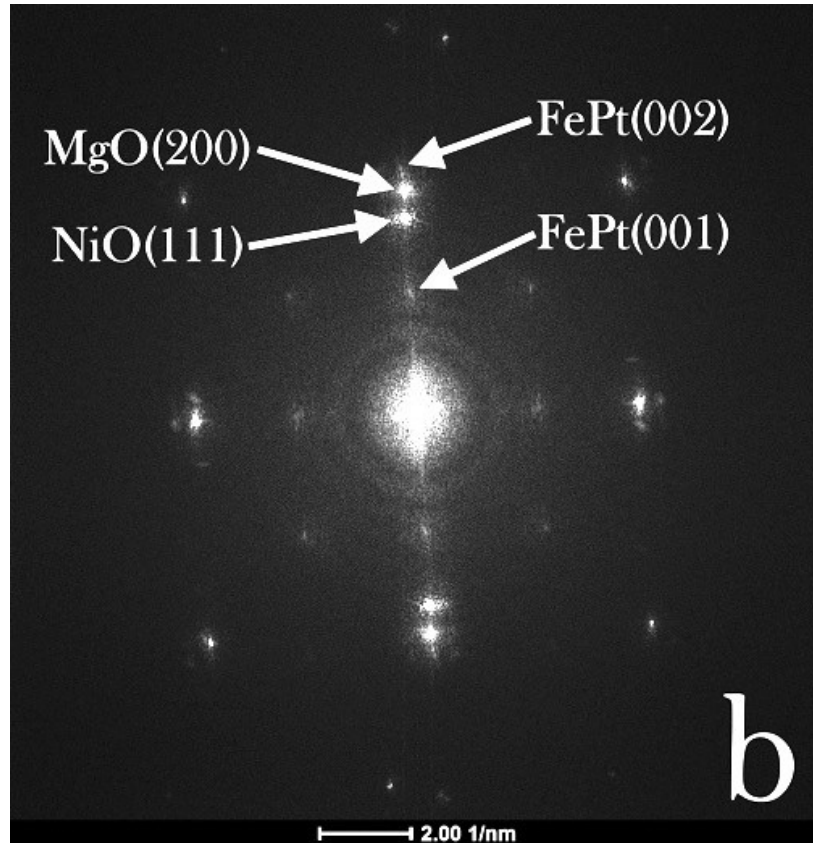


Figure 3: A FFT of Figure 2. Note the symmetry of the NiO (111) along the vertical axis and the epitaxial periodicity of the FePt spots along the vertical and horizontal axis

SQUID Magnetometry. The FC hysteresis loop data shown in Figure 4 for sample A and B were measured under the same conditions at 5K. The zero field cooled (ZFC) hysteresis loops were also measured from both samples under identical temperature (5K) and field conditions as the FC loops and were nearly identical to the FC curves aside from a small shift due the exchange bias effect. Both samples were measured in the perpendicular orientation due to the magnetocrystalline anisotropy of the FePt along the c axis of the epitaxial film. The large value of the cooling field (50 kOe) was applied during FC treatment to ensure all the Fe spins were saturated and so as to fully measure the exchange bias field. Although both samples have the same FePt layer thickness, a large difference in coercivity is observed in Figure 4. This can be explained

by the morphology of the FePt layer. Takahashi *et al.* have shown that the coercivity of FePt on MgO is highly related to the island size and morphology of the layer⁶. During deposition it is expected the hydrogen leaches the oxygen from the surface of the MgO leaving oxygen vacancies for Pt atoms to fill and nucleate for a more continuous FePt film⁵. An FePt layer with smaller grain size and separated island growth has a larger coercivity due to minimum magnetization cancelations at grain boundaries⁶. Conversely, an FePt layer with larger grain size and interconnected island growth exhibits a smaller coercivity due to the Fe spin cancelations resulting in a softer coercivity. The coercivity measured is 750 Oe and 5,700 Oe for sample A and B, respectively. Sample A exhibits an exchange bias value of $H_{EB} \approx -82$ Oe whereas sample B exhibits an exchange bias value of $H_{EB} \approx -40$ Oe. The full value of exchange bias is likely not exhibited in this study because it was not possible to heat the samples above Néel temperature of 523K of NiO prior to field cooling. The theoretical treatment offered by Kiwi *et al.* shows that may explain the compensated orthogonal FM/AFM coupling observed in our FePt/NiO bilayers. Because $H_{EB} \propto t_F^{-1}$, as long as the thickness of the ferromagnetic layer is thinner than the domain wall of the bulk FM wall $t_f < d_w^f$, then a reversible energy storage occurs in the incomplete domain wall formation in the FM layer³.

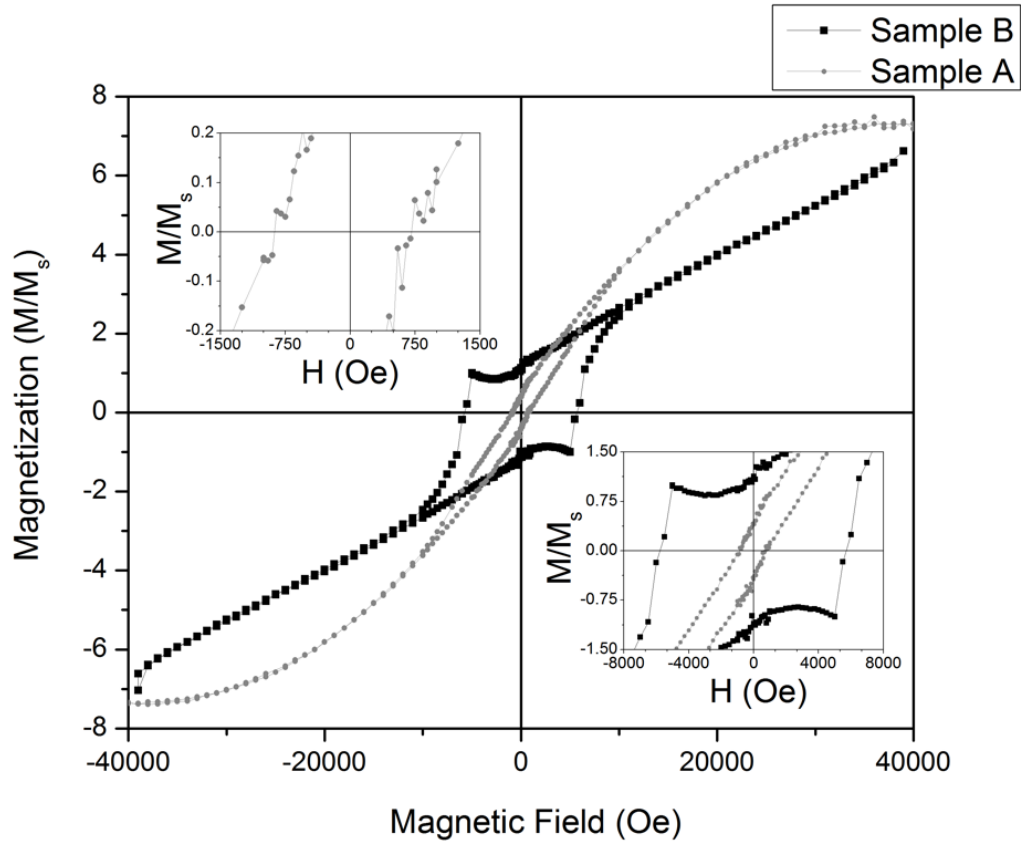


Figure 4: SQUID magnetometer data of sample A Sample B. Sample A exhibits soft-ferromagnetic properties. Sample B exhibits hard-ferromagnetic properties.

Conclusion

In conclusion, FePt was grown epitaxially on MgO with NiO grown highly oriented on top of the FePt layer under high vacuum and under low vacuum with forming gas atmosphere conditions. The MgO (100) and FePt (001) and NiO (111) planes are all parallel in the heterostructures as confirmed using XRD. The perpendicular exchange interface configurations between the Fe spins and the Ni spins give rise to perpendicular exchange bias confirmed using SQUID magnetometry hysteresis data. The FePt layer in both types of bilayer samples exhibits island like morphology. However, the thin film FePt/NiO bilayer sample grown under vacuum conditions exhibits considerably larger coercivity than the sample grown under partial pressure of forming gas, as observed from

FC hysteresis loop measurements made at 5 K. I explain this on the basis that the sample grown with a forming gas environment consists of a more continuous FePt film whereas the one grown under full vacuum conditions has an FePt film with smaller grain size and less interconnected islands. The FePt film having the smaller and less interconnected grains has considerably less Fe-Fe spin cancelations than the FePt with the more continuous grain structure, and therefore a greater coercivity.

Acknowledgements

I would like to deeply thank the graduate college of Missouri State University, the Wright-Patterson Air Force Base, and the MSU Physics, Astronomy and Materials Science faculty and my colleagues for all of their assistance and guidance in data acquisition and analysis.

References

- ¹ W.H. Meiklejohn and C.P. Bean, *Phys. Rev.* **105**, 904 (1957).
- ² M. Kiwi, J. Mejía-López, R.D. Portugal, and R. Ramírez, *Appl. Phys. Lett.* **75**, 3995 (1999).
- ³ M. Kiwi, *J. Magn. Magn. Mater.* **234**, 584 (2001).
- ⁴ T. Gao, N. Itokawa, J. Wang, Y. Yu, T. Harumoto, Y. Nakamura, and J. Shi, *Phys. Rev. B* **94**, (2016).
- ⁵ R. Maaß, M. Weisheit, S. Fähler, and L. Schultz, *J. Appl. Phys.* **100**, 073910 (2006).
- ⁶ Y.K. Takahashi, K. Hono, T. Shima, and K. Takanashi, *J. Magn. Magn. Mater.* **267**, 248 (2003).

MAGNETIC AND STRUCTURAL STUDY OF PERPENDICULAR MAGNETIC ANISOTROPY IN L₁₀ FEPT/NIO BILAYER THIN FILMS

Abstract

This article reports on the investigation of sub 10 nm FePt films with 100 nm of highly oriented NiO grown on top of the FePt. These films have been deposited in-situ using Pulsed Laser Deposition (PLD) on MgO (100) substrates. The key to this study is comparing 3 different films types that only differ by the growth pressure and atmosphere during the FePt deposition. These parameters are highly correlated with the morphology and structure seen in the 3 different film types. These films exhibit exchange coupling at the interface resulting in exchange bias seen in the SQUID magnetometry. This article presents a series of out-of-plane and in-plane magnetic measurements for an L₁₀ FePt/NiO bilayer. Parallel and perpendicular exchange bias is exhibited in this heterostructure. My XRD analysis shows that a well-ordered FePt layer having the L₁₀ phase has been deposited. Cross-sectional TEM FFT provides further evidence of the epitaxy of L₁₀ FePt and the highly oriented nature of NiO. HAADF images also acquired in the TEM show the island like morphology of the FePt layer. The film thickness is confirmed using XRR while also showing an atomic density distribution similar to the theoretical values for each layer.

Introduction

L₁₀ FePt is a leading candidate for high density perpendicular recording media. It shows promising potential in HAMR (heat assisted magnetic recording) and bit patterned

media^{1,2,3}. Growing an antiferromagnetic layer of on top of the ordered L1₀ has shown to induce perpendicular exchange bias (PEB) even up to room temperature⁴. Depending on the amount of PEB desired for the application, a hard or soft antiferromagnetic material can be grown on the FePt⁵. Examples for such antiferromagnetic materials having the requisite magnetic and structural properties to induce the desired amount of perpendicular exchange bias include FeMn or NiO^{4,6}. Exchange bias is not a required phenomenon for HAMR technology to be implemented, but FePt and its chemically ordered phase are leading candidates in the industry for high-density magnetic recording. Introducing exchange bias into this system can lead to interesting and unforeseen applications for the future. Exchange bias has already showed promising applications for spintronic applications such as MRAM (Magnetic Random Access Memory)^{7,8}. Exchange bias is important for many other spintronic applications^{9,10}. Although it may seem counterintuitive to couple such a strongly coercive magnetic material in bulk form, primarily because this can make it difficult to encode information, it is nevertheless useful to explore its properties in nanostructured heterostructure form due to the unexpected magnetic properties that may arise. Growing a weak antiferromagnetic material coupled with a strong ferromagnetic material should result in relatively small exchange bias compared to the coercivity of the ferromagnetic layer. In the new age of rapid technological advances and the need for miniaturization, nanostructure heterostructures containing magnetic materials need to be investigated in order to aid in the design of devices and in the development of fabrication processes to supply the demand for high quality magnetic devices.

Experimental

All films in this study were grown using pulsed laser deposition. All parameters to grow each layer have been previously optimized and then used to grow the bilayer structures presented here. The only difference between the three films presented in the study are the nanostructure and the crystalline structure of the FePt layer. To control the nanostructure and the crystallinity of these thin films the deposition gaseous atmosphere and vacuum pressure was adjusted and controlled to obtain the desired effects. The FePt layer of film A was grown in an atmosphere of forming gas (5% hydrogen & 95% argon) at the pressure of 1E-1 mbar in the vacuum chamber. Film B was deposited under high vacuum with the pressure in the chamber at 3.4E-6 mbar during the deposition. Film C contains an FePt layer that was deposited under argon gas at a chamber pressure of 1E-1 mbar. All FePt depositions were grown using a substrate temperature of 800°C. This is to induce the L1₀ ordering for the FePt. Subsequently, a 100 nm thick layer of NiO was deposited on the FePt layer of each of the films. Films A and C are similar in deposition parameters except for the crucial aspect that film C was not grown in the presence of any hydrogen. This resulted in radically different crystal structure in the FePt layer compared to that of films A and C.

The following describes the methodology used to synthesize the films: The MgO substrates were purchased from MTI Lab Co. The substrates were cleaned and one surface of each was epi-polished then packaged in a clean room before being shipped from the factory. The substrate was loaded into the vacuum chamber and pumped down to a base pressure of 1E-5 mbar. The substrate was heated under high vacuum up to 800°C and kept at this temperature for several hours to ensure the MgO substrate had

ample time to anneal and form a single crystal removing crystalline defects that may have been present. The deposition of the FePt layer for each sample was made using the FePt (50:50 at%) target and nanosecond pulses from the Nd:YAG pulsed laser. This laser produces a wavelength of 246 nm with a pulse width of 6 ns per pulse. A laser repetition rate of 10 Hz and a fixed amount of 10,000 shots were used to grow the FePt layer. During the deposition, the gas was held at constant pressure to create a uniform atmosphere during the deposition. Accordingly, for the high vacuum FePt deposition there was no gaseous atmosphere added during the deposition. After completion of the FePt layer deposition, the sample was cooled to 200°C in the environment that it was grown in. After the sample had equilibrated at 200°C, oxygen was introduced into the chamber to prepare for NiO deposition. For the NiO deposition, the oxygen pressure was held at 1.3E-2 mbar and the substrate temperature was held at 200°C. After the NiO layer deposition, the sample was cooled down to room temperature and the chamber was vented, whereupon the sample was removed for characterization. The difference between the film types A, B and C are the pressure and atmosphere used for the FePt layer growth.

Results and Discussion

X-ray Diffraction (XRD). Analysis of the XRD data presented in Figures 1 and 5 show that the FePt/NiO bilayer is highly oriented on the single crystal substrate for thin film samples A and B. Since the reflections from the FePt (001), (002) and (003) planes are clearly observed, this is a strong indication that the FePt layer is epitaxial with the MgO substrate¹¹. This is in agreement with previous studies showing that the L1₀ FePt and MgO have an epitaxial relationship¹¹. While NiO has been shown to have an

epitaxial relationship with $L1_0$ FePt⁴, the XRD data presented in Figures 1 and 5 do not show this unambiguously. The XRD data for film A is presented in Figure 1. The XRD pattern for the film A, with FePt grown under a low vacuum of forming gas (5% H₂ and 95% Ar) atmosphere, shows very similar XRD data as obtained for film B. The XRD reflections (i.e., peaks in the XRD data) from FePt (001), (002) and (003) and NiO (111) planes are present at the same angles for films A and B. Figure 5, which presents the out-of-plane XRD data for the FePt/NiO film B, is consistent with the FePt layer in this film being grown under high vacuum of 3.4E-6 mbar resulting in a sharp MgO/FePt interface.

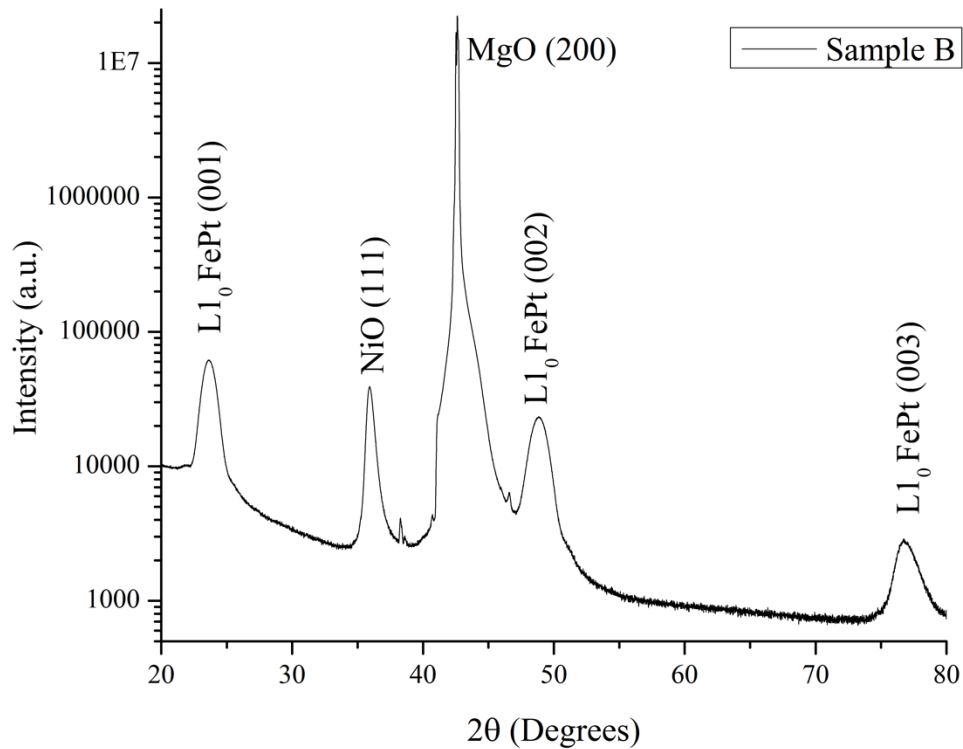


Figure 5: XRD Measurements of Sample B. This Shows the epitaxial nature of the $L1_0$ FePt layer and the highly oriented NiO layer. The XRD for film type A looks very similar to this figure.

The XRD pattern for film C (Figure 6) with FePt grown under a low vacuum of argon atmosphere shows a significantly different XRD pattern. No $L1_0$ FePt peaks are present in the entire scan. The only peaks that are observed is the MgO substrate peak and a single A1 FePt peak. The A1 phase of FePt is chemically disordered and only exhibits one peak in figure 6 suggesting that this layer has some preferential orientation. There are no NiO peaks in this scan suggesting this layer is amorphous on top of the A1 FePt layer. This is a stark difference compared to the XRD data discussed above for films A and B. The A1 phase of FePt also exhibits no magnetocrystalline anisotropy as the Fe atoms and Pt atoms are distributed in the FCC lattice in a random fashion¹². The close proximity of the MgO and FePt (200) peaks suggests that the FePt layer is textured and has preferred orientation. To confirm epitaxy, in plane lattice measurements are required.

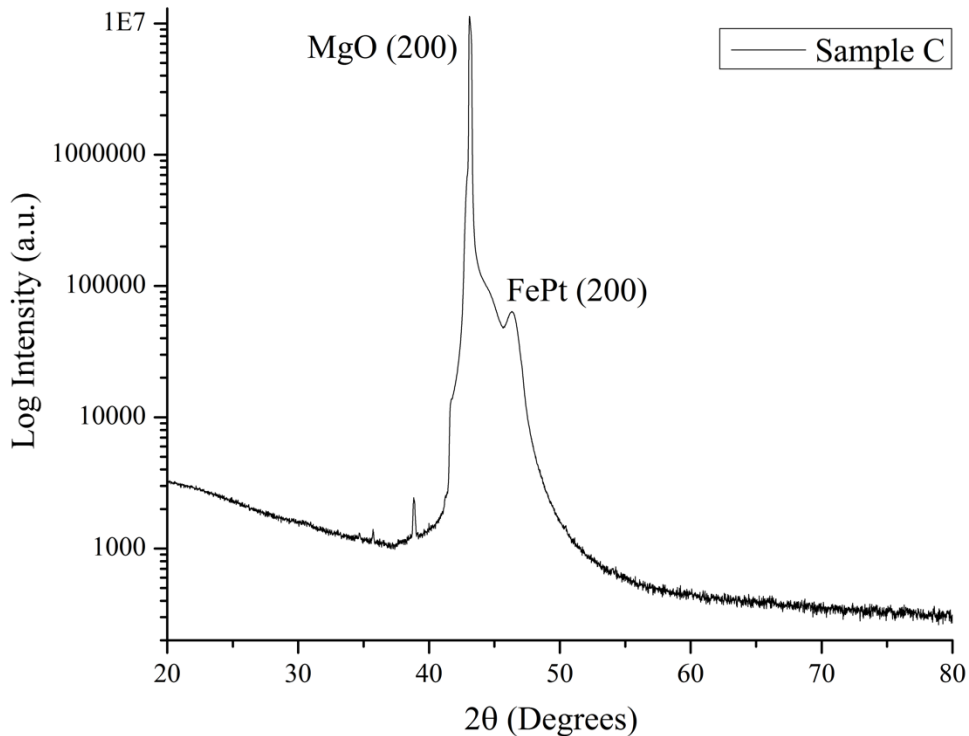


Figure 6: XRD measurements of the film type C. The FePt (200) peak is the A1 phase

High-Angle Annular Dark Field Imaging (HAADF). HAADF imaging gives a deeper understanding of the crystalline nature present in the NiO layer. Although NiO and FePt have a known epitaxial relationship, HAADF imaging has also been shown to detect crystalline defects in the NiO layer⁴. Similarly, the HAADF image of film A shown in Figure 7 indicates that the NiO layer is not perfectly epitaxial but is nevertheless highly oriented with respect to the surface of the FePt layer. The HAADF images show the FePt as very bright due to its high Z-contrast. HAADF imaging is very sensitive to the samples Z-contrast. A HAADF image is formed by only very high angle, incoherently scattered electrons by Rutherford scattering where the electron beam is scattered from the nucleolus of the atoms in the sample. These HAADF images also show the island growth of the FePt layer. This is expected due to the high lattice mismatch between the FePt and the MgO substrate. It has also been shown previously that the size of these FePt islands can be controlled by adjusting the vacuum pressure and gaseous atmosphere during the deposition¹³. Growing FePt in a low vacuum in the presence of forming gas should result in a more continuous and interconnected FePt layer whereas growing FePt in a high vacuum environment with no gas added results in smaller and more separated¹⁴. The control of the FePt island size using forming gas or high vacuum has been well documented¹⁵.

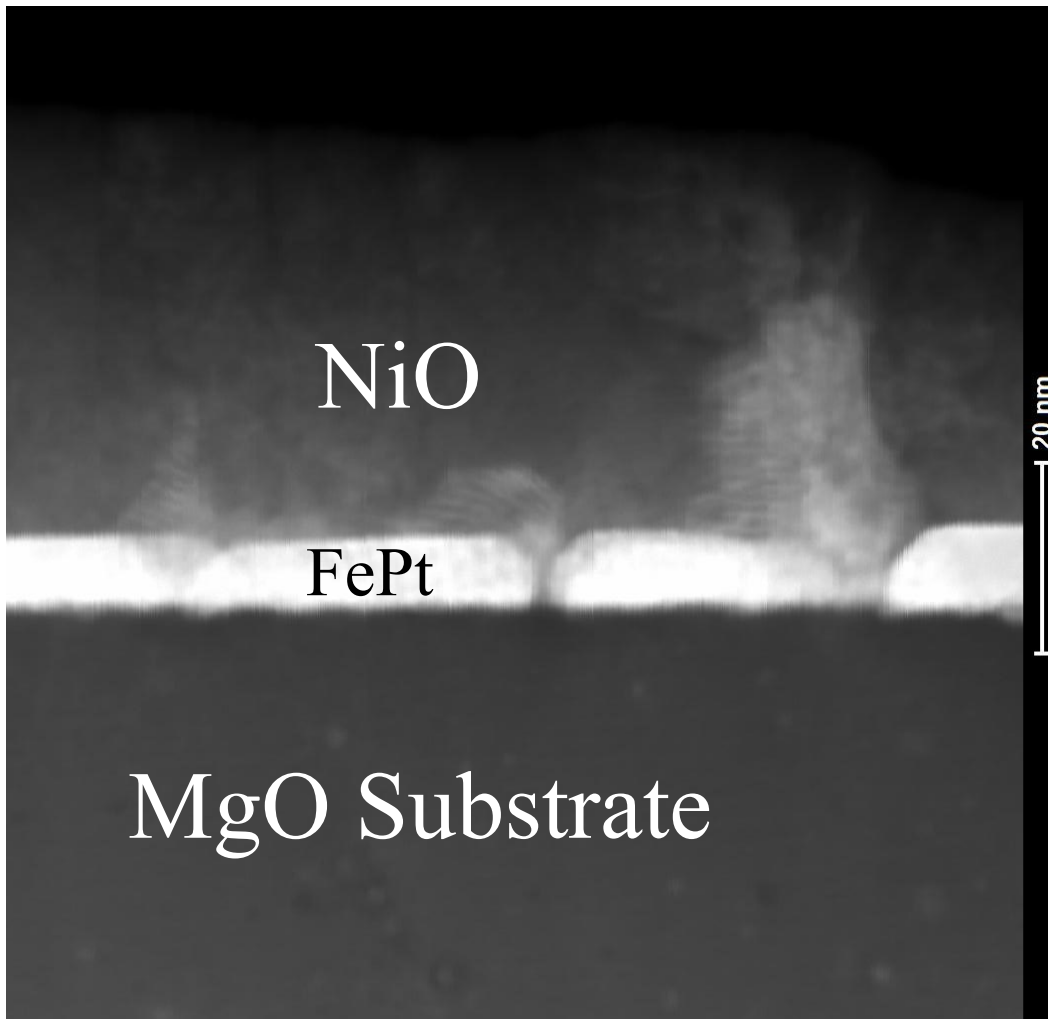


Figure 7: HAADF image of film type A. The bright islands are $L1_0$ FePt while the material on top of the is the highly oriented NiO. Note the scale bar on the right.

The scale bar on the right hand side of the TEM HAADF micrograph shown in Figure 7 has been used to estimate the thickness of the FePt layer. Using this scale bar, it was determined the FePt layer is roughly 7 nm thick. Although the NiO layer extends much above this micrograph, from a separate TEM image it was confirmed that the NiO layer was roughly 105 nm in thickness.

Energy Dispersive X-ray Spectroscopy Mapping (EDS). Energy dispersive x-ray spectroscopy was used in the transmission electron microscope to confirm the

elemental content of the thin film samples. The mapping function of the EDS software is very useful to map and overlay elemental colored mapping images. This was used to map the elemental content of the thin films in sample A. The overlaid EDS mapping can provide information on the distribution of the elements in a cross section of a thin film sample. The deconvoluted data shows that all of the appropriate elements (Fe, Pt, Ni, O, Mg) are distributed accordingly within their respective layers with very minimal to no inter-diffusion that may potentially occur during the high temperature growth of the FePt/NiO bilayer. The substrate shows strong indication that magnesium and oxygen are present which is appropriate as the substrate is MgO. The next layer, iron platinum, shows a strong signature of Fe and Pt, which is appropriate for this layer. It appears there may be a trace amount of oxygen in this layer from the EDS map but this is likely on top or on the bottom of the thinned TEM sample and not actually a part of the grown layer. This is consistent with the fact that the FePt layer was grown in forming gas or at a high vacuum where only an extremely insignificant amount of oxygen is present¹³. In addition, the XRD presents no Fe or Pt oxide peaks and the magnetic properties of these films are preserved. This suggests the FePt layer is not oxidized. The island growth of the FePt is also seen in the EDS maps and is discussed in depth in the HAADF section. The next layer, NiO, shows strong signals of Ni and O which is expected for this layer. Figure 8 is an image showing the convoluted EDS mapping of film type A. Note the difficulty in resolving the composition of the individual layers. However, this is easily resolved by deconvolution as shown in Figure 9. Figure 9 is a collection of the individual, deconvoluted EDS mapping images from the thin film sample A.

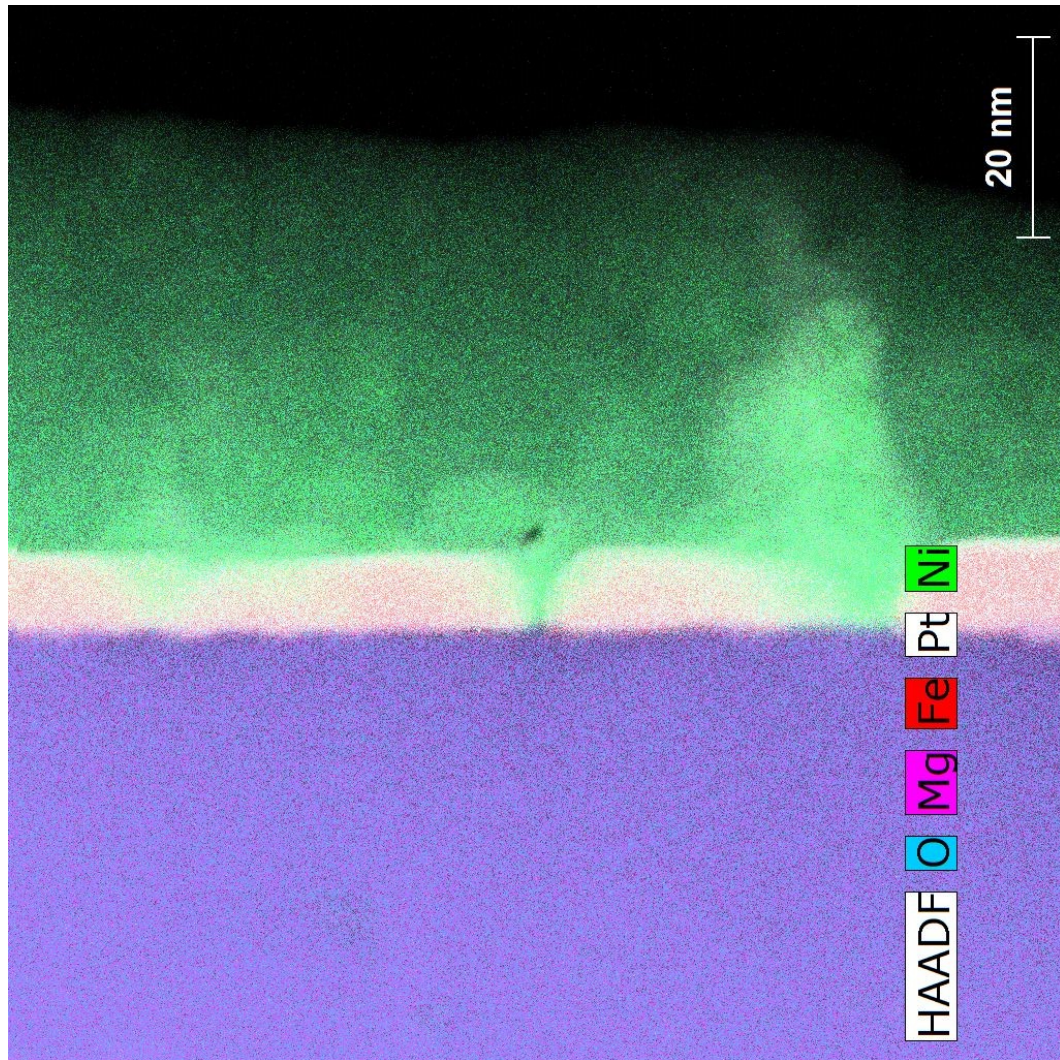


Figure 8: EDS of the sample type A. Note the difficulty in resolution even with the drastically different colored elements.

The top left image in Figure 9 is the HAADF image that was obtained and presented above as Figure 7. The top right image shows the Ni EDS map of the cross section of sample A. The middle left image shows the Fe EDS map whereas the middle right image shows the Pt EDS map.

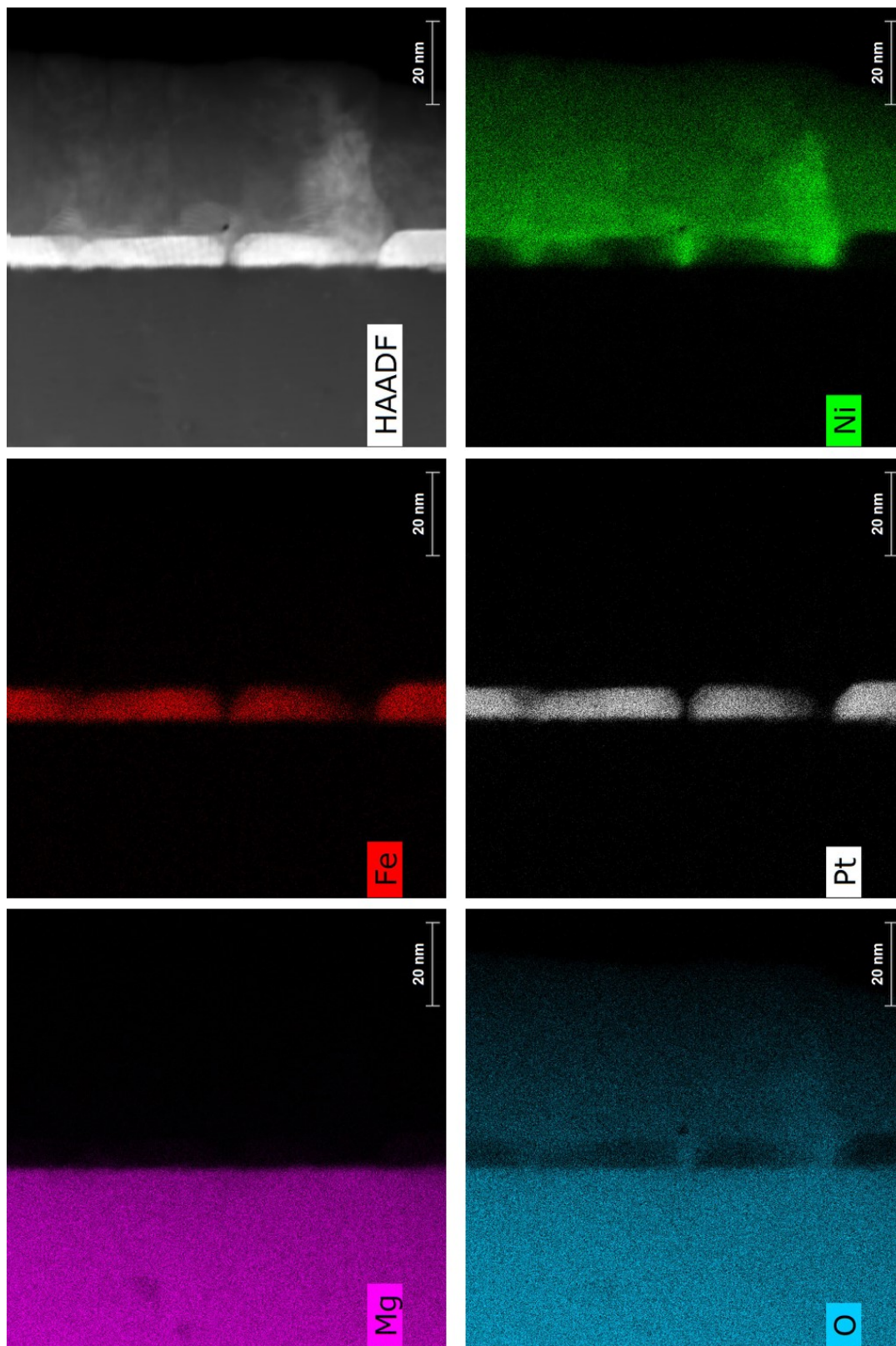


Figure 9: The separated images of figure 8 (sample A). Note the FePt island seen in the middle images.

The bottom left and bottom right images show the Mg and O EDS maps of the cross section of sample A. Quantization of elements is possible with using EDS but can be somewhat inaccurate if the detector is not calibrated for the material present in the scan.

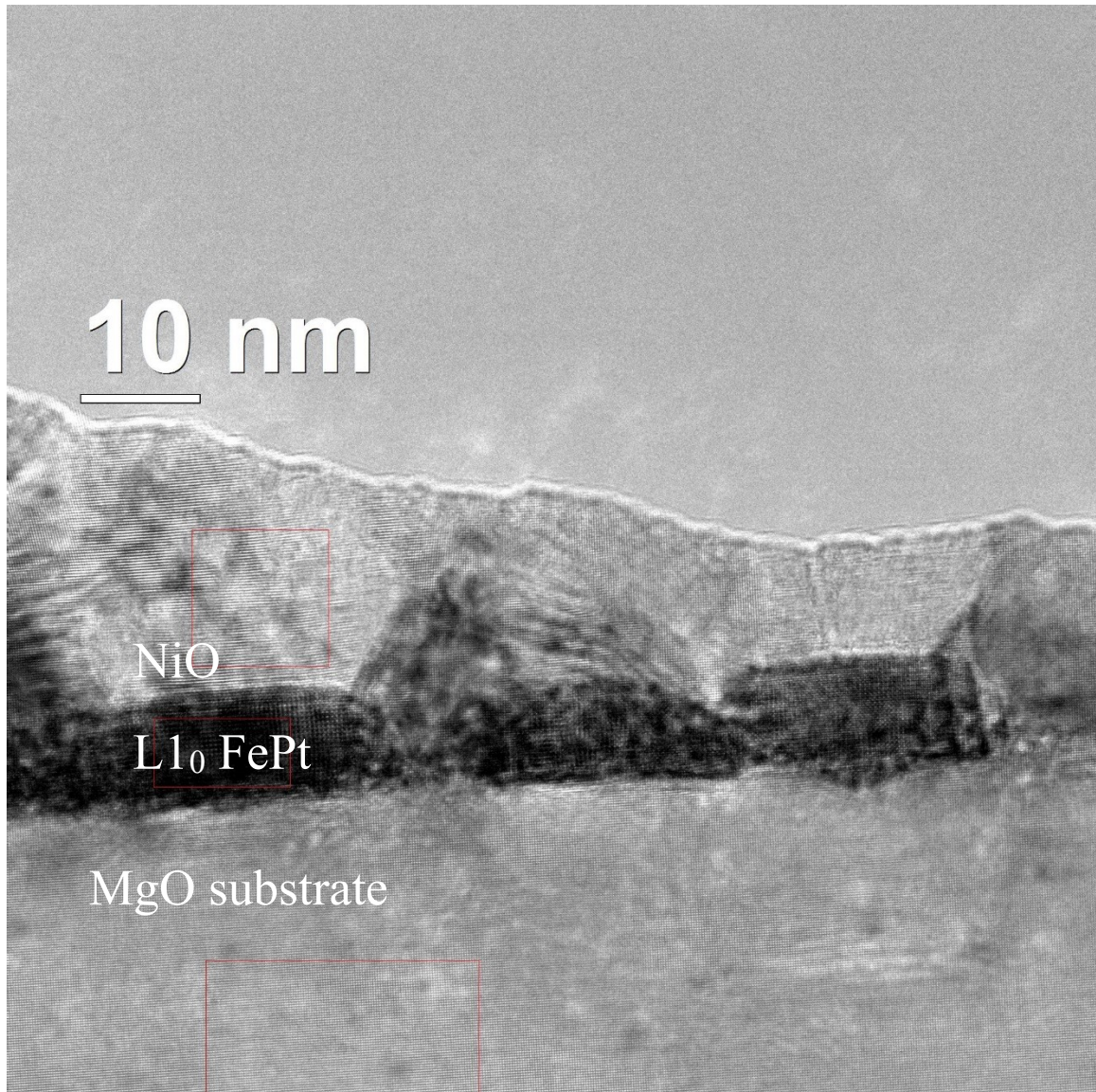


Figure 10: High-resolution TEM Micrograph of Sample type A. Note the grains/islands of FePt and the NiO crystalline dislocations. The scale length bar is 10 nanometers.

Fast-Fourier Transform (FFT) of TEM Micrograph. The fast-Fourier transform (FFT) has also been taken of the high magnification TEM micrograph (Figure 10) and is shown in Figure 11. Figure 10 is the result of many hours of sample preparation and TEM microscope time. This TEM lamella was created using a FIB-SEM and thinned until it became electron transparent. The lamella was further cleaned in a NanoMill to remove the amorphous gallium layer. This resulting micrograph (Figure 10) is likely the pinnacle of my MSU graduate studies. This micrograph proves the bilayer nature of the film. The multiple domains of NiO are also observed, but over each FePt island is a well ordered domain of NiO. It is suspected this domain of NiO is epitaxial with the FePt island.

Figure 11 expresses in-plane crystallographic information of the grown bilayer. The crystallographic planes are labeled to denote the origin of the reciprocal lattice plane. Figure 11 shows the FFT of the entire TEM image shown in Figure 10. This FFT shows the crystallinity of a given material but instead, mapped out in reciprocal space. The overlapping lattice diffraction spots can make it difficult to resolve the different materials involved in the bilayer structure. The FFT of the entire micrograph can be deconvoluted by just selecting a specific area (of a uniform grain) in each thin film layer to take the fast-Fourier transform. The results from such selective analysis are shown in Figure 12. The FFT of just the FePt layer shows the cubic tetragonal structure. This is expected as $L1_0$ FePt is a FCT cubic structure¹⁶. Since the FFT is mapped in reciprocal (to real) space, the C-axis is compressed whereas the a/b axis is expanded as expected. The 2D periodic nature of the FePt FFT proves the epitaxy of FePt layer on the MgO substrate¹⁷.

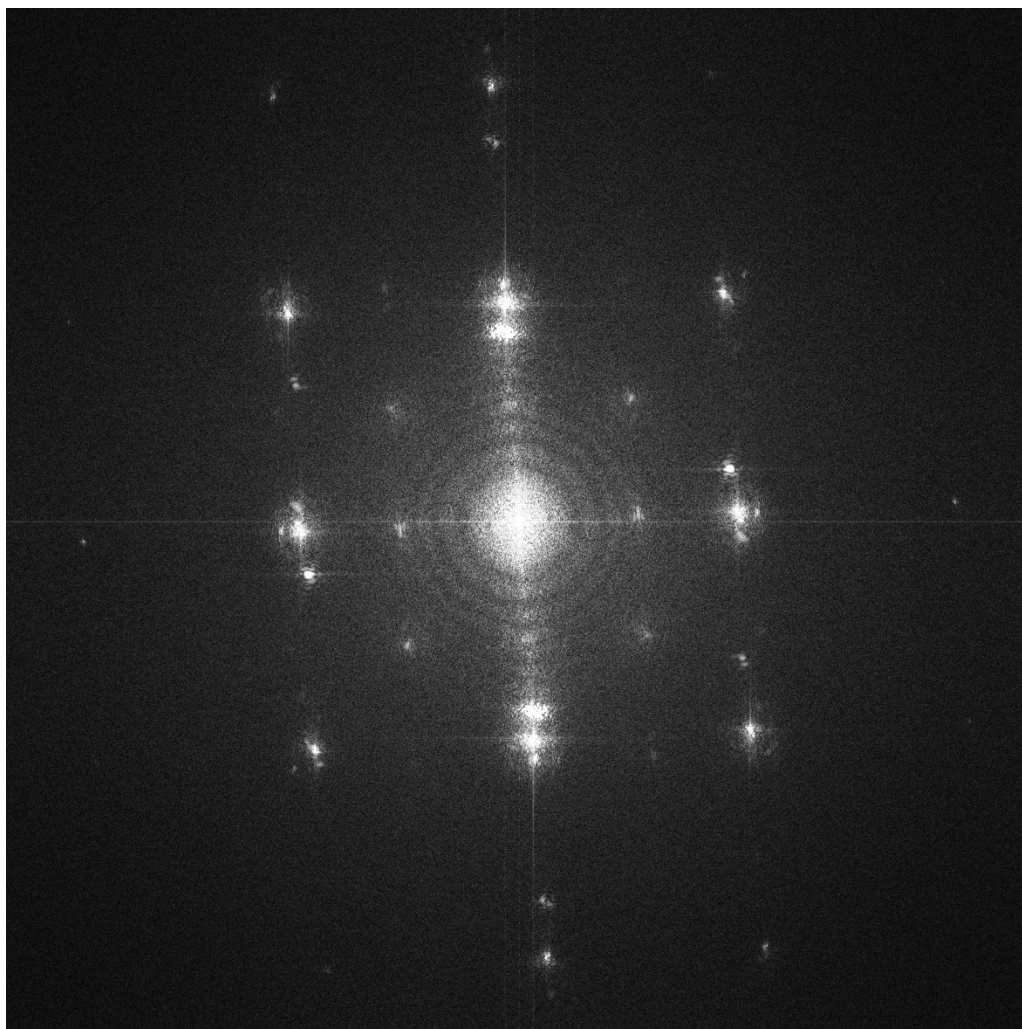


Figure 11: Fast-Fourier transform of Figure 10 high-resolution micrograph.

To further elaborate on this, since the FFT is in reciprocal space, the lattice compression and elongation actually indicates that the c axis is elongated in real space and the a and b axes are compressed in real space of the $L1_0$ FePt layer. The FFT of the NiO layer shows a periodic nature along the perpendicular axis to the substrate coinciding with reflections from the NiO (111) planes. This NiO (111) planes are parallel to the substrate, as observed from the XRD data. The NiO layer likely has epitaxial registry with the FePt layer because of the NiO (222) peak seen in extended XRD scans. This has been calculated and the six-fold symmetry has been observed in other published work⁴. The

epitaxy of the NiO is not seen here because the NiO lattice is not aligned with the microscope. This is seen in Figure 12 in the FFT of the NiO layer. The slight angle seen in the FFT images is due to the slight tilt in the single crystal substrate. It can be seen that the single crystal substrate exhibits very sharp and bright simulated diffraction points.

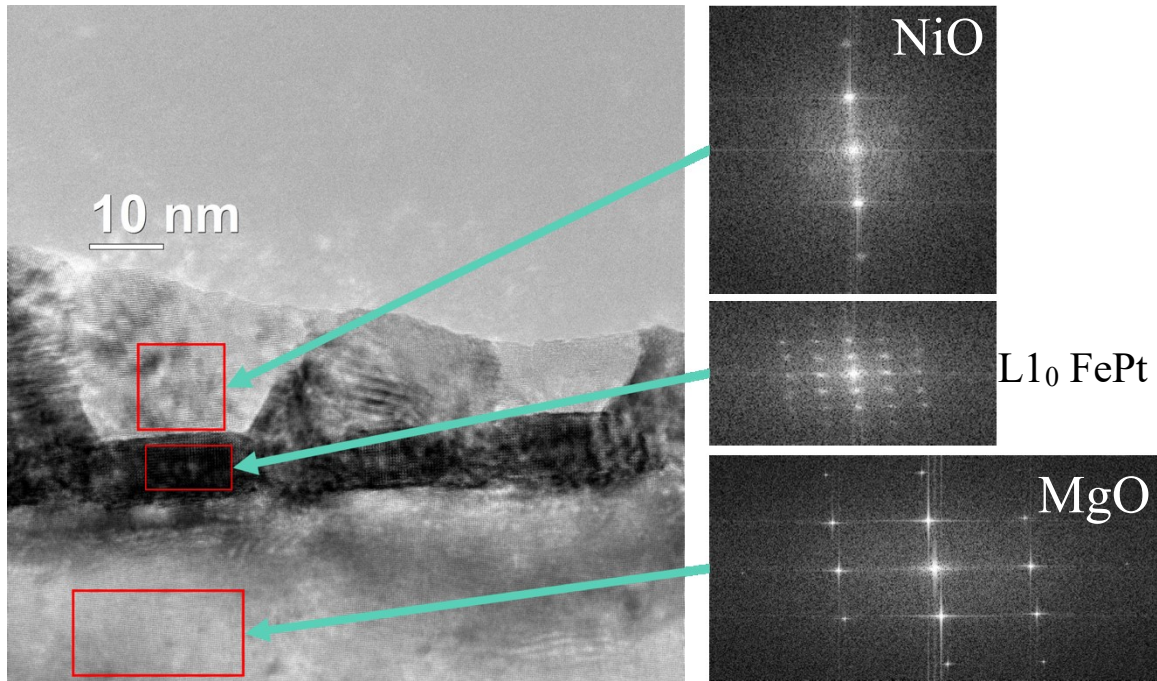


Figure 12: The separated FFT of the High-magnification TEM micrograph from sample A

X-Ray Reflectivity (XRR). XRR is similar to XRD because both use Bragg's law to form constructive and deconstructive wave interference that results in the diffraction pattern seen in Figure 13. The main difference is that the angle scanned during the XRR measurement is much smaller than in XRD. For XRR to give information about the layer thickness and density of multiple layers in thin films, the scan is typically performed from zero degrees to ten degrees. According to Bragg's law, using the traditional Cu Ka-1 radiation results in a diffraction pattern on the order of the layer's

thickness in a thin film. This typically ranges from sub-1nm to hundreds of nanometers¹⁸. This diffraction pattern encodes the information about the thicknesses of each of the individual layers in the sample. The periodic spacing between the peaks having a unique phase in 2-theta is analyzed to determine the thickness of a particular layer in the thin film sample. The broader/wider the peaks, the thinner that layer is. Alternatively, if the diffraction pattern oscillations are very narrow and sharp, this indicates a thicker layer is present.

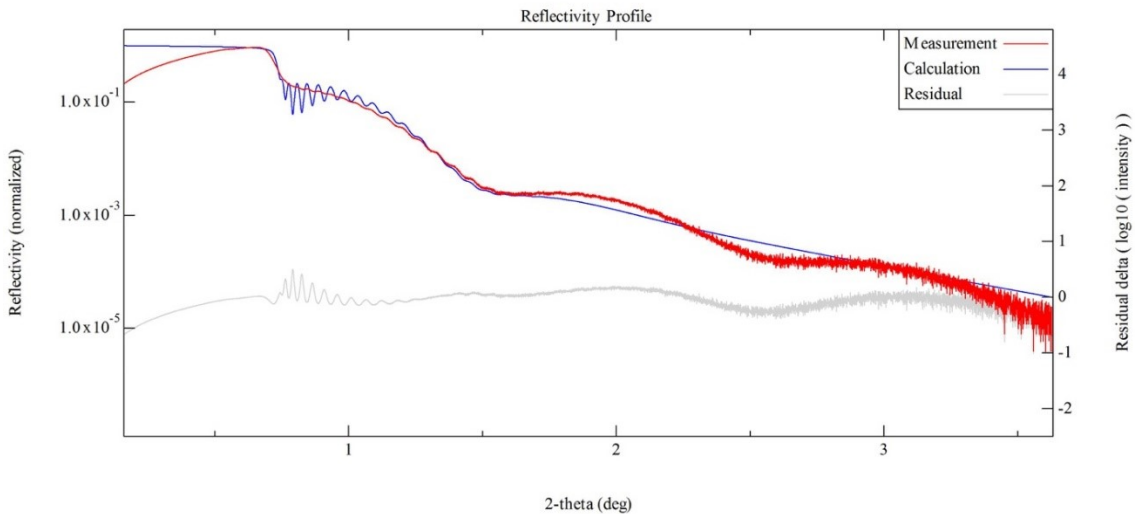


Figure 13: XRR of Sample A. The experimental data is in red, the calculated XRR pattern is in blue and the residual signal is in grey.

The overall sloping large diffraction peaks shown in Figure 13 correspond to reflections from the FePt layer whereas the small-superimposed oscillations correspond to the reflections from the NiO layer. Although these values can be calculated by hand, a program was used to fit the data to give the most accurate calculation for the scan collected. The measured diffraction patterned is shown in red and the calculated fitted pattern is shown in blue in Figure 13. The analysis from this fitting is shown in Figures

14 and 15. Figure 14 is a density distribution graph which plots the density vs. depth of the film in nanometers. This gives insight to the calculated density of each layer from the fitted XRR curve. These densities agree fairly closely with the theoretical atomic densities known for FePt and NiO^{19,20}.

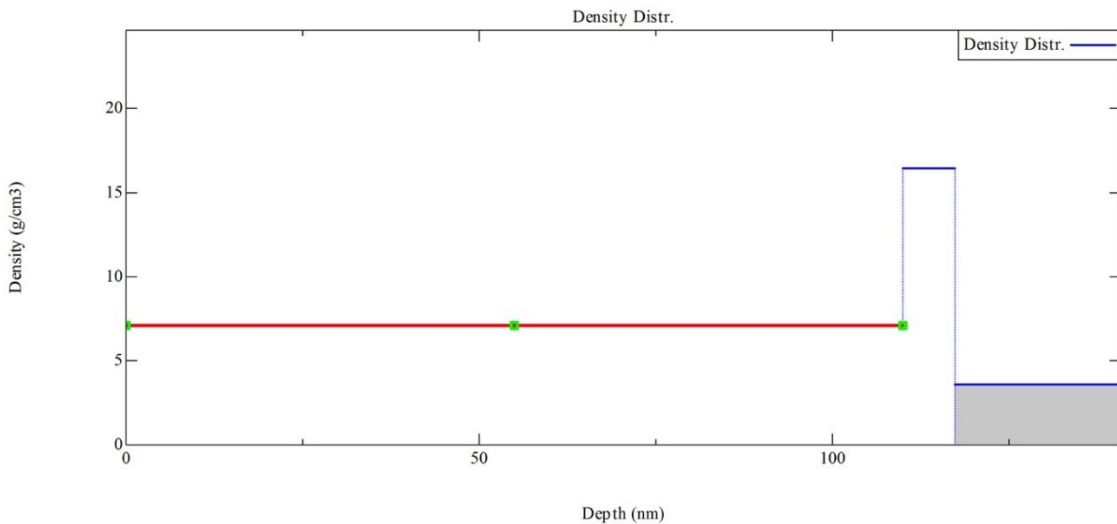


Figure 14: The density distribution function of film type A calculated from the XRR diffracted intensities peaks.

Another result obtained from the XRR data analysis is the film block diagram shown in Figure 15. This includes an illustration of the film with the film thickness and densities indicated in the diagram. The thickness measurements have been enlarged to provide clarity. The XRR fitting software was used to calculate the thickness of the FePt film to be 7.36 nm with a density of 16.43 g/cm³ and a surface roughness of 1.99 nm. Similarly, the thickness of the NiO film was estimated to be 109.97 nm with a density of 7.092 g/cm³ and a surface roughness of 2.89 nm.

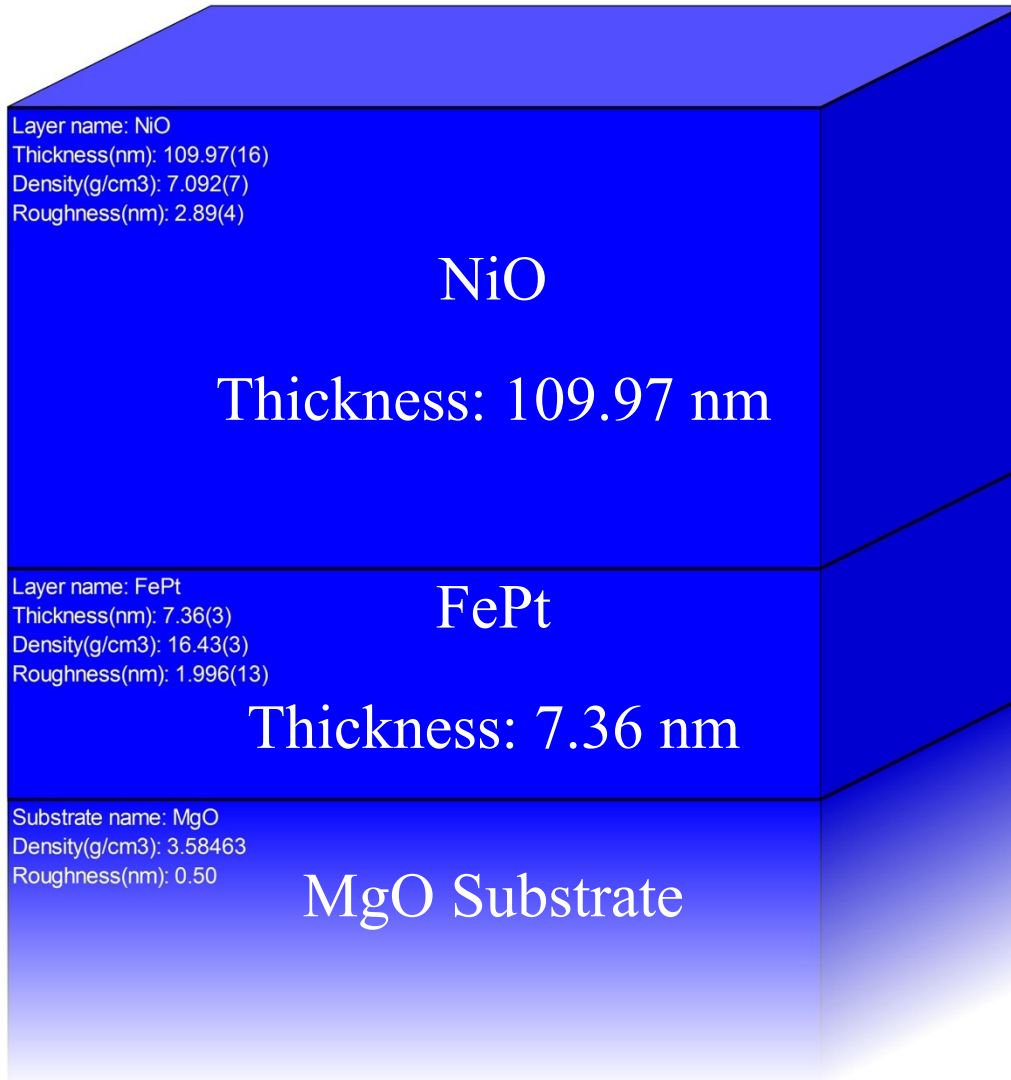


Figure 15: The film block diagram of film A with quantified properties calculated from the XRR experimental measurement. This includes film thickness, density, and surface roughness.

SQUID Magnetometry. To measure the exchange bias, a field cooled (FC) and a zero field cooled (ZFC) M-H hysteresis loop must be measured. The shift of the FC loop along the H-axis, or the applied field axis, is the exchange bias present in a sample²¹. Magnetometry measurements for all thin films were conducted in a superconducting quantum interference device magnetometer. M-H curves were generated for film types A,B and C in both in-plane orientation and out-of-plane orientation. To exhibit partial

exchange bias in the bilayer thin films all films were field cooled from 300K to 5K under a magnetic field of 50kOe (it is necessary to heat the sample above the Néel temperature of the AFM layer in order to measure the full extent of the exchange bias field). This field cooling procedure is necessary to orient the individual spins in the FM and AFM layers, in order to detect the exchange bias present in the sample. The Néel temperature of nickel oxide, the antiferromagnetic material present in all samples, is roughly 523K²². SQUID magnetometers are rarely designed to reach such high temperatures for magnetic measurements. To sufficiently measure all exchange bias in these films it is necessary to field cool these samples from 530K to 300K in a vacuum furnace with an applicable magnetic field. Due to the lack of access to such a furnace, all samples were field cooled from 300K to 5K. This leads to only a partial display of exchange bias this system is capable of exhibiting. Since the same field cooling parameters were followed for each sample it is appropriate to compare the exchange bias found in these samples as a side-by-side comparison.

The in-plane vs. out-of-plane measurements present a method of investigating the magnetocrystalline anisotropy and exchange bias in different directions of the thin film sample. A highly chemically ordered epitaxial thin film of L1₀ FePt will exhibit a large magnetic anisotropy along the c-axis, the [001], direction of the thin film. This is due to the face centered tetragonal cubic structure of the chemically ordered L1₀ phase. The compression of the L1₀ FePt unit cell along the a and b lattice edges results in the elongation of the c axis. In this chemically ordered phase, layers of iron and platinum alternate along the c-axis²³. This gives rise to strong magnetic coupling between the iron atoms and thus leads to the high magnetocrystalline anisotropy along the c-axis²⁴. Due to

the epitaxial relationship of MgO and L1₀ FePt this magnetic anisotropy points in the normal direction to the surface of the substrate, MgO (001)²⁵.

NiO has a very interesting antiferromagnetic structure. NiO is antiferromagnetic due to the sheets of nickel atoms in the family of (111) planes in the bulk NiO²⁶. The planes of nickel atoms are antiparallely aligned and therefore results in a zero net magnetic spin. NiO also has an epitaxial relationship with L1₀ FePt. In this epitaxial relationship the NiO (111) plane is parallel with the L1₀ FePt (001) plane⁴. This leads to a unique magnetic interface between the FePt and the NiO. The iron atoms in the L1₀ FePt have a magnetic moment normal to the sheets of nickel in the NiO (111) planes. This results in a net ferromagnetic moment pointing perpendicular to the antiferromagnetic spins⁴. Exchange bias is measured in such a sample in the out-of-plane orientation is known as perpendicular exchange bias^{6,27}.

Figures 16-21 show the M-H curves for thin film samples A,B and C. Each thin film has also been measured in the in-plane and out-of-plane orientation resulting in six M-H hysteresis loops. The physical significance of each of the M-H hysteresis loops will be discussed below. Figure 16 is the in-plane M-H hysteresis loop for sample type A. The coercivity shown in Figure 16 is relatively smaller than the one for the hysteresis loop measured in the out-of-plane condition for the same sample (Figure 17). This difference in coercivity is explained by the magnetocrystalline anisotropy of L1₀ FePt film. Figure 16 also exhibits an exchange bias value of approximately $E_B = -57$ Oe. Figure 17 shows the M-H hysteresis loop of sample A but as measured in the out-of-plane orientation. Figure 17 yields an exchange bias value of $E_B = -82$ Oe. This difference in exchange bias is not yet understood completely.

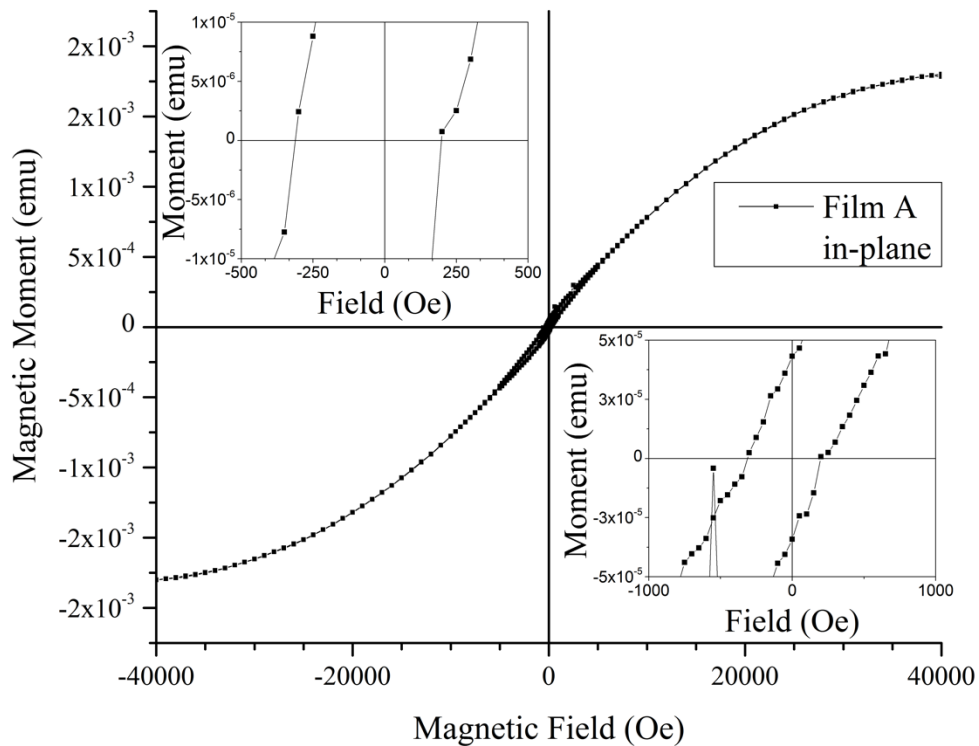


Figure 16: Magnetic M-H hysteresis loop of film A in the in-plane orientation.

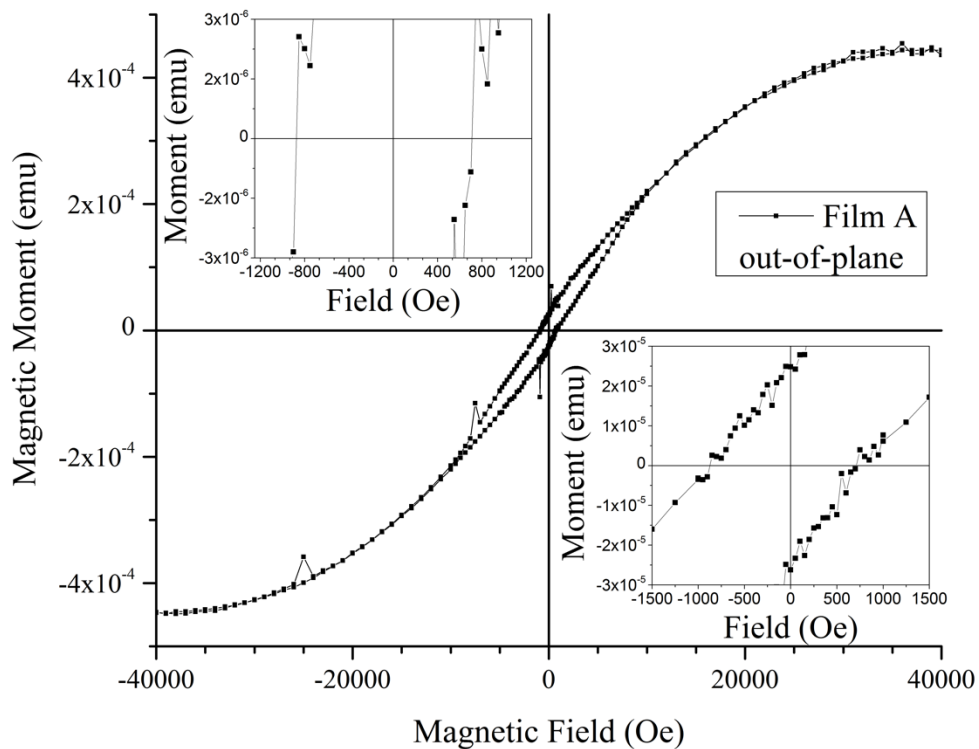


Figure 17: Magnetic M-H hysteresis loop of film A in the out-of-plane orientation.

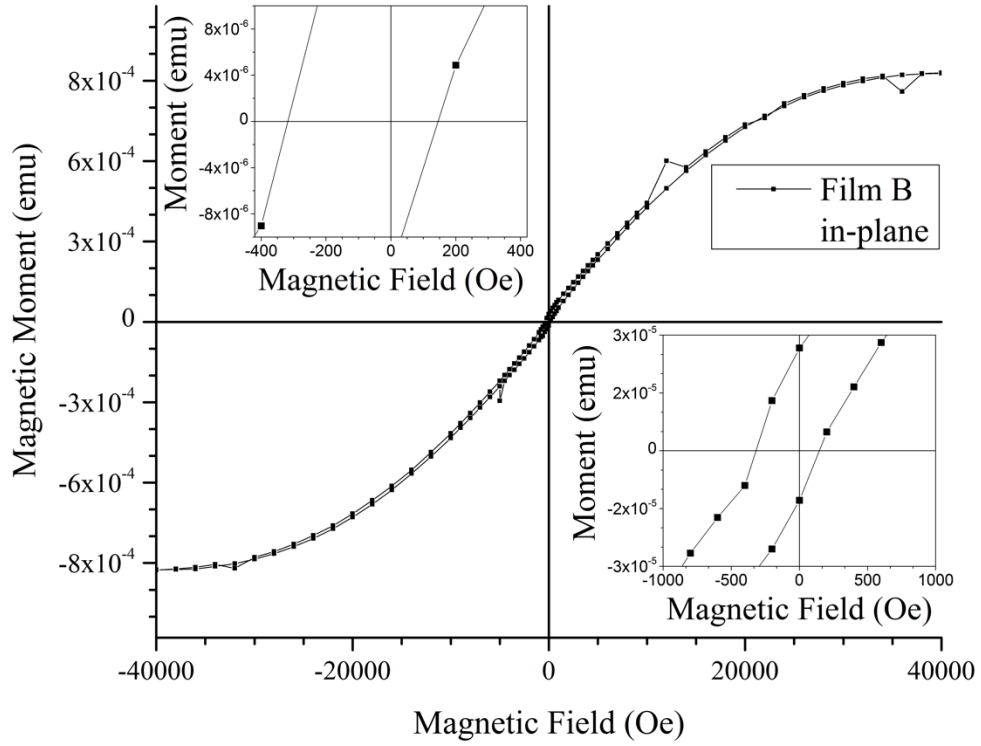


Figure 18: Magnetic M-H hysteresis loop of film B in the in-plane orientation.

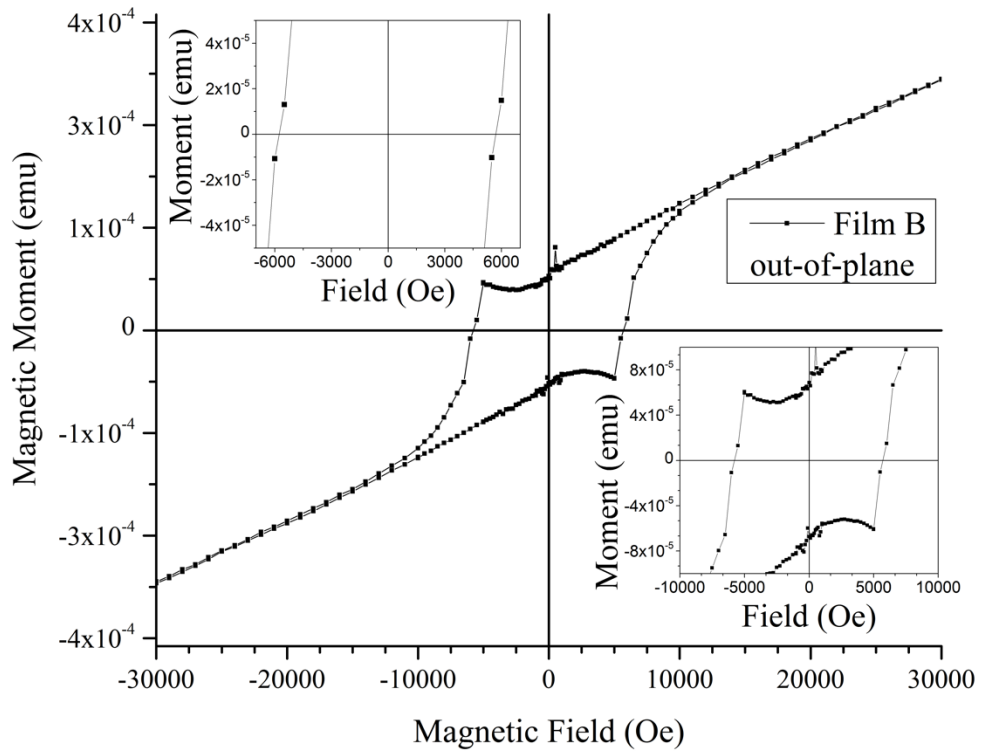


Figure 19: Magnetic M-H hysteresis loop of film B in the out-of-plane orientation.

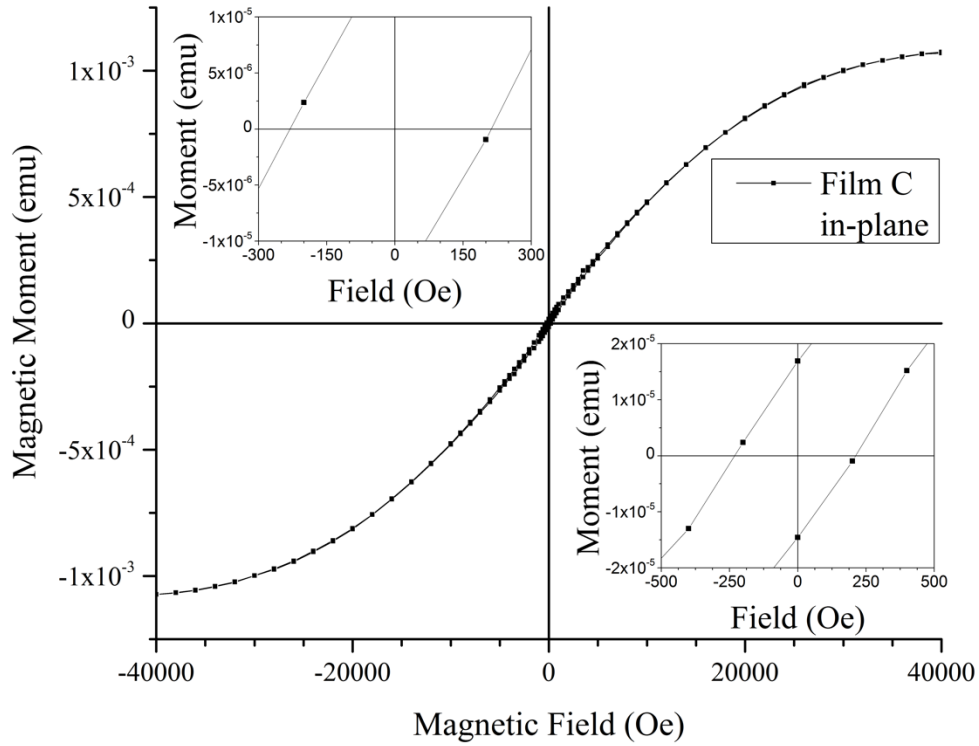


Figure 20: Magnetic M-H hysteresis loop of film C in the in-plane orientation.

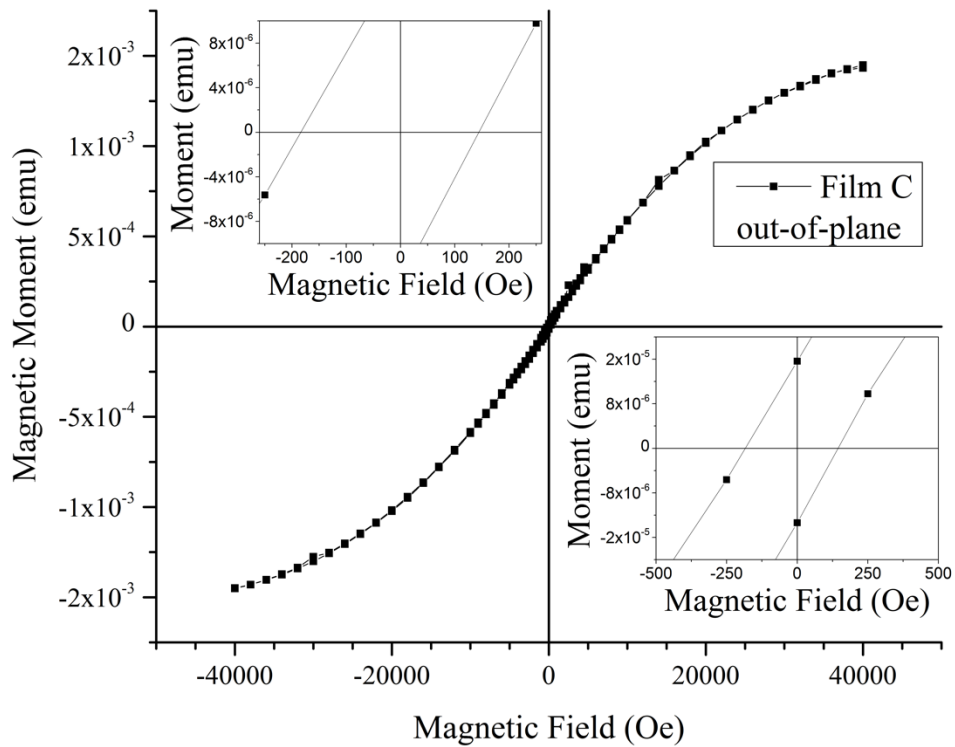


Figure 21: Magnetic M-H hysteresis loop of film C in the out-of-plane orientation.

Sample B exhibits a coercivity that is considerably larger than that of sample A, showing that it has a very high magnetocrystalline anisotropy normal to the film's surface. This is consistent with the results from the XRD measurements discussed above. The XRD shows very sharp $L1_0$ FePt peaks indicating the layer is highly chemically ordered, thus resulting in a high magnetic anisotropy along the c-axis. As shown in Figures 18 and 19, the in-plane exchange bias is approximately -85 Oe whereas the out-of-plane E_B is approximately -40 Oe for sample B, respectively.

Sample C exhibits no magnetic anisotropy. This is due to the A1 phase of the FePt layer, which has an equal chance for Fe or Pt to occupy a given site in the lattice (i.e., not a chemically ordered phase). This results in a random distribution of Fe and Pt in the lattice and creates an FCC lattice. Because the lattice parameters $a = b = c$ in the FCC lattice, there is no tetragonal elongation and no magnetic coupling of Fe in the chemically ordered Fe layers. This results in an isotropic M-H hysteresis loop. This is in agreement with the XRD measurements of sample C. In this case, there are no $L1_0$ FePt peaks detected in the scan; instead only one A1 FePt peak (200) is present. The exchange bias as measured from the in-plane hysteresis loop shown in Figure 20 is approximately -10 Oe whereas E_B measured from the out-of-plane hysteresis loop shown in Figure 21 is approximately -20 Oe. The SQUID data have not been background subtracted so it appears it takes such a large field to saturate the magnetization. However, this is actually due to the antiferromagnetic layer of NiO. This AFM layer produces a linear M-H graph that can be background subtracted to result in the appropriate saturating M-H curve for the entire thin film sample.

Conclusions

Film B exhibits the highest magnetocrystalline anisotropy of all three films while film C exhibits no anisotropy. This is consistent with the XRD data measured the thin film samples. The average FePt layer thickness is around 7 nm while the NiO seen to have a thickness of just over 100 nm. The TEM HAADF micrographs show the crystalline defects present in the NiO layer and the high Z contrast of the FePt layer. FFT of the high magnification TEM confirms the epitaxy of the FePt layer and shows that the NiO overlayer highly oriented in the bilayer structure. XRR was used to determine the thickness of each thin film layer, which was found to be in agreement with the estimates obtained from the TEM micrographs, and the atomic density for each layer. Although small, the exchange bias values observed for the thin film samples are promising considering the samples were not heated above the Néel temperature prior to field cooling. The differences observed in the exchange bias values for the in out-of-plane vs the in-plane M-H measurements are not well understood. In addition, a complete theory for exchange bias has yet to be presented. Most likely, a combination of creative sample synthesis, characterization and either computational or theoretical modeling are required to provide a more complete understanding of the exchange bias in nanostructured materials.

References

- ¹ D. Weller, G. Parker, O. Mosendz, A. Lyberatos, D. Mitin, N.Y. Safonova, and M. Albrecht, *J. Vac. Sci. Technol. B Nanotechnol. Microelectron. Mater. Process. Meas. Phenom.* **34**, 060801 (2016).
- ² J. Hu, K.M. Cher, B. Varghese, B. Xu, C. Lim, J. Shi, Y. Chen, K. Ye, J. Zhang, C. An, and W. Tsai, *IEEE Trans. Magn.* **52**, 1 (2016).
- ³ B.S.D.C.S. Varaprasad, Y.K. Takahashi, and K. Hono, *JOM* **65**, 853 (2013).
- ⁴ T. Gao, N. Itokawa, J. Wang, Y. Yu, T. Harumoto, Y. Nakamura, and J. Shi, *Phys. Rev. B* **94**, (2016).
- ⁵ L. Suber, P. Imperatori, E.M. Bauer, R. Porwal, D. Peddis, C. Cannas, A. Ardu, A. Mezzi, S. Kaciulis, A. Notargiacomo, and L. Pilloni, *J. Alloys Compd.* **663**, 601 (2016).
- ⁶ N.N. Phuoc and T. Suzuki, *J. Appl. Phys.* **101**, 09E501 (2007).
- ⁷ L. Frangou, K. Akmalidinov, C. Ducruet, I. Joumard, B. Dieny, and V. Baltz, *Phys. Procedia* **75**, 1058 (2015).
- ⁸ I.L. Prejbeanu, M. Kerekes, R.C. Sousa, H. Sibuet, O. Redon, B. Dieny, and J.P. Nozières, *J. Phys. Condens. Matter* **19**, 165218 (2007).
- ⁹ W. Zhang and K.M. Krishnan, *Mater. Sci. Eng. R Rep.* **105**, 1 (2016).
- ¹⁰ M.B. Jungfleisch, W. Zhang, and A. Hoffmann, *Phys. Lett. A* **382**, 865 (2018).
- ¹¹ P. Lupo, J. Orna, F. Casoli, L. Nasi, P. Ranzieri, D. Calestani, P. Algarabel, L. Morellón, and F. Albertini, *EPJ Web Conf.* **40**, 08001 (2013).
- ¹² G. Giannopoulos, T. Speliotis, W.F. Li, G. Hadjipanayis, and D. Niarchos, *J. Magn. Magn. Mater.* **325**, 75 (2013).
- ¹³ R. Maaß, M. Weisheit, S. Fähler, and L. Schultz, *J. Appl. Phys.* **100**, 073910 (2006).
- ¹⁴ M. Carbucicchio, R. Ciprian, and G. Palombarini, *J. Magn. Magn. Mater.* **322**, 1307 (2010).
- ¹⁵ M. Nakaya, M. Kanehara, M. Yamauchi, H. Kitagawa, and T. Teranishi, *J. Phys. Chem. C* **111**, 7231 (2007).
- ¹⁶ S. Noda, Y. Tsuji, A. Sugiyama, A. Kikitsu, F. Okada, and H. Komiyama, *Jpn. J. Appl. Phys.* **44**, 7957 (2005).

- ¹⁷M. Futamoto, M. Nakamura, T. Shimizu, M. Ohtake, and T. Shimotsu, *IEEE Trans. Magn.* **1** (2018).
- ¹⁸M.F. Toney and S. Brennan, *J. Appl. Phys.* **66**, 1861 (1989).
- ¹⁹J.M. Vargas, R.D. Zysler, L.M. Socolovsky, M. Knobel, and D. Zanchet, *J. Appl. Phys.* **101**, 023903 (2007).
- ²⁰X. Wang, L. Qiao, X. Sun, X. Li, D. Hu, Q. Zhang, and D. He, *J. Mater. Chem. A* **1**, 4173 (2013).
- ²¹J. Nogués and I.K. Schuller, *J. Magn. Magn. Mater.* **192**, 203 (1999).
- ²²F.B. Lewis and N.H. Saunders, *J. Phys. C Solid State Phys.* **6**, 2525 (1973).
- ²³J.P. Liu, K. Elkins, D. Li, V. Nandwana, and N. Poudyal, *IEEE Trans. Magn.* **42**, 3036 (2006).
- ²⁴S. Ayaz Khan, P. Blaha, H. Ebert, J. Minár, and O. Šipr, *Phys. Rev. B* **94**, (2016).
- ²⁵A. Kohn, N. Tal, A. Elkayam, A. Kovács, D. Li, S. Wang, S. Ghannadzadeh, T. Hesjedal, and R.C.C. Ward, *Appl. Phys. Lett.* **102**, 062403 (2013).
- ²⁶A. Schrön, C. Rödl, and F. Bechstedt, *Phys. Rev. B* **86**, (2012).
- ²⁷C. Binek, P. Borisov, X. Chen, A. Hochstrat, S. Sahoo, and W. Kleemann, *Eur. Phys. J. B* **45**, 197 (2005).

SUMMARY

I have successfully grown an epitaxial bilayer of $L1_0$ FePt/NiO on a single crystal substrate of MgO. The growth of $L1_0$ FePt is confirmed by XRD, SQUID and the FFT of the cross sectional TEM. It is difficult to form a completely chemically ordered layer of $L1_0$ FePt. The results put forward in this thesis suggest the FePt layer is highly chemically ordered in the $L1_0$ phase for films A and B. This allows the NiO to grow on top of the FePt in a highly ordered fashion. There is a known epitaxial relationship for NiO and FePt. The XRD suggests the NiO may be epitaxial due to the high ordered reflections of NiO (222), but this claim is not confirmed in this thesis. In the TEM, the NiO lattice is only aligned with along the out-of-plane axis. This gives proof for the highly oriented NiO layer, but falls just short of supporting the epitaxial NiO claim. The XRR was used to provide the thicknesses and atomic densities of each layer from the calculated diffraction pattern. Growing $L1_0$ and A1 phases of FePt has given an interesting perspective of studying the magnetic anisotropy and its correlation with perpendicular exchange bias present in the FePt/NiO bilayer system. As predicted, growing these phases of FePt and coupling it with an interface of antiferromagnetic NiO has resulted in different in-plane and out-of-plane values for exchange bias. The exchange bias that occurs at the magnetic interface of FePt/NiO bilayer is still not well understood. Several theorists have presented promising solutions for complete calculations of exchange bias that have applications to specific cases. However, a unified theory of the exchange bias effect that is sample independent still eludes us. The combination of experimental measurements and theoretical calculations of the exchange bias effect present a bright future for spintronics and other magnetic applications.